

Testing the performance of ice thickness models to estimate the formation of potential future glacial lakes in Austria

Jan-Christoph Otto¹  | Kay Helfricht²  | Günther Prasicek^{1,3}  |
Daniel Binder^{4,5}  | Markus Keuschnig⁶ 

¹Department of Geography and Geology, University of Salzburg, Salzburg, Austria

²Institute for Interdisciplinary Mountain Research (IGF), Austrian Academy of Sciences (ÖAW), Innsbruck, Austria

³Interdisciplinary Center for Mountain Research (ICMR), University of Lausanne, Sion, Switzerland

⁴Climate Research Section, Central Institute for Meteorology and Geodynamics ZAMG, Vienna, Austria

⁵Glaciology and Climate Department, Geological Survey of Denmark and Greenland (GEUS) Copenhagen, Denmark

⁶GEORESEARCH Forschungsgesellschaft mbH, Puch bei Hallein, Austria

Correspondence

Jan-Christoph Otto, University of Salzburg, Department of Geography and Geology, Hellbrunnerstr. 34, 5020 Salzburg, Austria.
Email: jan-christoph.otto@sbg.ac.at

Funding information

Austrian Academy of Sciences

Abstract

The emergence of glacial lakes is a significant consequence of global climate change in high mountain regions. Recent developments in ice thickness modelling combined with high-resolution glacier surface data led to the generation of modelling approaches to simulate the ice-free bedrock topography below current glaciers and to detect potential glacier bed overdeepenings (GBO) that may form into future lakes. We simulated the subglacial topography in the Austrian Alps using two different ice thickness models. Glaciers in the study area differ significantly from glaciers investigated in previous studies on potential future lakes because of their in general small size and location often restricted to cirques. The aim of this study is to estimate the number and location of potential future lakes in Austria. We tested the performance of ice thickness models for modelling of potential future lakes in an environment dominated by mountain glaciers that are under high stress of climate change. Modelling results are compared with lakes that evolved since the modelling periods and with data on subglacial topography derived from geophysical surveys. Results show significant differences in model performance concerning the total ice volume and the number of simulated GBOs. The number and total area of the modelled GBOs is overestimated, compared with the number of lakes that have evolved in the past. Most GBOs are simulated for valley type glaciers, even though most glaciers are mountain types. This does not match with the location of existing glacial lakes that are dominantly found in cirques. We ascertain that this modelling approach performs better on large valley type glaciers and less well on mountain glaciers. Intersecting the modelling runs indicates that up to 42 new lakes may form within 23 glaciers in Austria covering a total area of 2 km².

KEYWORDS

Austrian Alps, climate change, future lakes, Glacial Lakes, glacier-bed overdeepening, ice thickness modelling

1 | INTRODUCTION

The European Alps, like most mountain environments, are experiencing significant landscape changes as a response to ongoing climate change. Glacier mass loss in the twentieth and early twenty-first century is the most visible manifestation of these changes, leading to the exposure of new terrain, an increase in loose sediment deposits and

the reduction of ice and water resources in high alpine regions. One consequence of glacier melt is the formation of glacial lakes (Carrivick & Tweed, 2013; Haeberli et al., 2016). Glacial lakes form in bedrock depressions, or behind dams of debris or ice. They are frequent landscape elements in glaciated mountain environments. Lakes that form in high mountain environments have significant impacts on sediment transfer, hydrology and society, for example through the

This is an open access article under the terms of the Creative Commons Attribution-NonCommercial License, which permits use, distribution and reproduction in any medium, provided the original work is properly cited and is not used for commercial purposes.

© 2021 The Authors. *Earth Surface Processes and Landforms* published by John Wiley & Sons Ltd.

formation of hazards (Haeblerli et al., 2017; Otto, 2019). Due to their potential to create hazardous glacial lake outburst floods (GLOFS), they are in focus of geomorphological research in many high mountain areas (Clague & O'Connor, 2015; Kapitsa et al., 2017; O'Connor & Costa, 2004). While in contact with ice, glacier lakes feed back positively on the glacier system, resulting in increased ice velocities, impacts on mass balances and enhanced melting (King et al., 2019; Sutherland et al., 2020). Recent insights also highlight their role as carbon sink due to their low organic carbon content and the high amount of fine sediments that are available for CO₂-consuming chemical weathering (Pierre et al., 2019).

An increasing number of new lakes and growth of existing glacier lakes have been reported from various mountain regions around the globe (Buckel et al., 2018; Cook et al., 2016; Emmer et al., 2016; Laute & Beylich, 2021; Mergili et al., 2013; Pandey et al., 2021; Pelto et al., 2013; Song et al., 2016; Wilson et al., 2018; Zhang et al., 2015). Recent developments in ice thickness models combined with high-resolution glacier surface data led to the generation of approaches to simulate the future, ice-free bedrock topography below current glaciers (Frey et al., 2010b; Gharehchahi et al., 2020; Linsbauer et al., 2012; Pandit & Ramsankaran, 2020; Paul & Linsbauer, 2012). The analysis of these modelled glacier beds reveals subglacial bedrock depressions, termed glacier bed overdeepenings (GBO), that represent potential locations for future lakes (Cook & Swift, 2012). Based on the assumption that the shape of the glacier surface reflects the bedrock surface beneath the glacier, a subtraction of the ice thickness from the glacier surface produces a potential subglacial morphology. Paul and Linsbauer (2012) back up this assumption by postulating that current glaciers contribute less to bedrock erosion compared with glaciers during the major glaciations. Consequently, current glaciers rather flow on the previously carved bedrock surface, thus portraying the bedrock morphology. An alternative to modelling ice thickness explicitly is to analyse morphometric conditions and surface characteristics of the glacier surface and estimate the potential for the location of GBOs by selected criteria (Colonia et al., 2017; Frey et al., 2010a). These criteria include slope < 5°, increasing slope in flow direction, formation of crevasses, or a reduction in glacier width. This alternative requires a mostly manual classification of glacier morphology and thus does not allow predictions on large scales. Modelling of potential GBOs has been performed for selected mountain regions and even large ice shields (for example: Gharehchahi et al., 2020; Kapitsa et al., 2017; Linsbauer et al., 2013; Livingstone et al., 2013; Pandit & Ramsankaran, 2020; Viani et al., 2020).

The most frequent ice thickness model used to predict potential future lakes is the GlabTop model generated by Linsbauer and others (2009) and further developed by Paul and Linsbauer (2012). A fully automated version of GlabTop is presented as GlabTop2 by Frey and others (2013). While the original GlabTop approach requires the manual definition of branch lines, GlabTop2 uses random points for ice thickness calculation. Thus, GlabTop2 seems to be better suited for an assessment of GBOs in entire mountain ranges with a high number of glaciers. GlabTop and GlabTop2 have been applied to model potential GBOs in Switzerland (Linsbauer et al., 2012), the Himalaya-Karakorum region (Allen et al., 2016; Linsbauer et al., 2016; Pandit & Ramsankaran, 2020; Ramsankaran et al., 2018; Zhang et al., 2019), the Djungarskiy Alatau, Kasachstan/China border (Kapitsa

et al., 2017), the Peruvian Andes (Colonia et al., 2017; Drenkhan et al., 2019), the Mont Blanc Area (France, Magnin et al., 2020) and the Aosta Valley in Italy (Viani et al., 2020).

To assess the quality of GBO simulations, modelled GBOs are compared with potential GBO locations based on the glacier morphology mentioned above (Frey et al., 2010a). Frequently, alternative ice thickness models are applied to compare location and geometry of GBOs (e.g. ITEM, Farinotti et al., 2009); HF-Model, Huss & Farinotti, 2012; or Volta, James & Carrivick, 2016). Ice thickness and GBOs are evaluated using field data derived from geophysical surveys. The accuracy of GlabTop and GlabTop2 with respect to the modelled ice thickness lies within a range of $\pm 30\%$ (Linsbauer et al., 2012, 2016), which is in accordance with the many other existing ice thickness models (Farinotti et al., 2017). Another way to validate modelling results is by comparing predicted lakes with lakes that have evolved in recent times. This requires topography data of previous glacier extents and an inventory of lakes (Kapitsa et al., 2017; Linsbauer et al., 2012; Viani et al., 2020). Similarly, the performance of modelling subglacial topography can be assessed by utilising older glacier inventories to model the subglacial topography of now ice-free areas (Viani et al., 2020). Most studies conclude that the models applied generate robust predictions with respect to the location of potential GBOs but information on lake size or depth contains a high degree of uncertainty (Magnin et al., 2020; Viani et al., 2020).

This study complements the picture of potential future glacial lakes in mountain environments by modelling GBOs at glaciers of the Eastern Alps in Austria. The composition of glaciers in the study area differs significantly from most of the regions where the modelling of potential future lakes has been performed previously (Colonia et al., 2017; Kapitsa et al., 2017; Magnin et al., 2020; Ramsankaran et al., 2018). The Eastern Alps in Austria are significantly lower compared with the Western Alps (Switzerland, France) or the Central Asian or Andean mountain regions, with maximum elevations below 4,000 m (Sommer et al., 2020). Ninety percent of all glaciers in Austria are smaller than 1 km² and account for 34% of the total glacier area (Fischer et al., 2015b). Seventy-five glaciers (9%) have an area between 1 and 5 km² and covering 41% of the total glacier area. The ten largest glaciers are between 5 and 12 km² in area and share 25% of the glacier cover and about 35% of the total glacier volume in Austria (Fischer et al., 2015b; Helfricht et al., 2019). Glaciers in the Austrian Alps are mostly mountain glaciers like cirque and niche glaciers (Cogley et al., 2010), with only a few typical valley glaciers (Otto et al., 2018). Furthermore, all glaciers have experienced strong melt leading to significant reduction in glacier size, a notable decrease in flow velocity and frequent split-up into small parts (Fischer et al., 2015b; Fleischer et al., 2021; Stocker-Waldhuber et al., 2019). We assume that mountain glaciers experience different mass turnover and flow dynamics, compared with valley glaciers, due to their small size, reduced thickness and lower shear stress (Capt et al., 2016; DeBeer & Sharp, 2009; Florentine et al., 2020; Paasche, 2011; Sanders et al., 2010). However, theoretical approaches of the ice thickness models are mainly based on flow behaviour (driving stress) or mass conservation, which are predominantly tested and calibrated against data from large glaciers. In general, ice thickness models estimate total glacier volume within a range of $10 \pm 24\%$ compared with measured thickness (Farinotti et al., 2017). The aim of the study is to

test the performance of two ice thickness models on the simulation of GBOs. We assess the sensitivity of modelling parameters on the number and characteristics of GBOs and estimate the location and dimensions of potential future lakes in Austria. We discuss the performance of ice thickness models for modelling of potential future lake locations in an environment dominated by mountain glaciers that are under high stress of temperature warming.

The objectives of this study are:

1. To model the location and size of GBOs in order to assess the potential locations and characteristics of potential future glacial lakes in high mountain areas of Austria.
2. To compare the performance of two different ice thickness models, namely GlabTop2 (Frey et al., 2014) and the HF-model (Huss & Farinotti, 2012), and to assess the sensitivity of modelled GBOs on model choice.
3. To compare the modelled GBOs of past glacier extents with existing lakes in order to evaluate model uncertainties and the estimated number of potential future lakes.
4. To validate the modelling results against ice thickness and bedrock surface data derived by high-resolution geophysical surveys.
5. To discuss the performance of the models applied with respect to glacier types observed in the Austrian Alps.

2 | STUDY SITE

We performed this study in the Austrian Alps, Europe (Figure 1). The Austrian part of the Eastern Alps represents around one-third of the

European Alps, covering an area of roughly 53,000 km². Around 8,000 km² of the Austrian Alps are located at altitudes above 2,000 m, setting the stage for the formation of more than 900 individual glaciers. The highest density of glaciers can be found in the Ötztaler Alps and the Venediger and Großglockner range. Austrian glaciers have lost more than 70% of area since the Little Ice Age (LIA) covering 330 km² in 2015 (Buckel et al., 2018). Glacier melt thus uncovered more than 600 km² of high alpine terrain. Between 2006 and 2016, Austrian glaciers lost about 22% of their volume (Helfricht et al., 2019). Since the onset of warming in mid-nineteenth century, more than 260 lakes have formed in the proglacial zone (Buckel et al., 2018).

3 | METHODS AND DATA

3.1 | Modelling glacier ice thickness and deriving subglacial depressions

We compare two different ice thickness models for the automated detection of future glacier lakes: GlabTop2 (Frey et al., 2014) and the HF model (Helfricht et al., 2019; Huss & Farinotti, 2012). The general approach to identify GBOs is to model the ice thickness, which is then subtracted from the ice surface to obtain the subglacial topography. Within the simulated subglacial topography, GBOs are detected using GIS analysis techniques (see below). The method only allows predicting glacier lakes forming in bedrock depressions without accounting for lakes that may form behind moraine dams. GBO modelling was performed for two different glacier extents, 1969 and

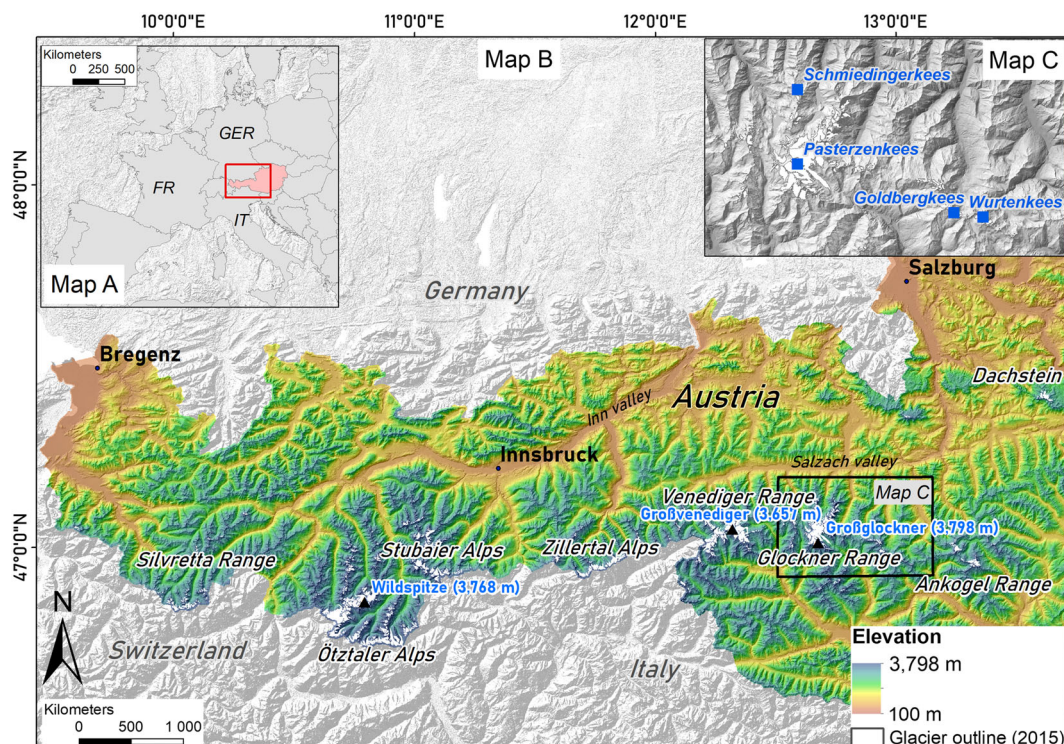


FIGURE 1 The study focusses on glaciers in the Austrian Alps, Europe (Map A). Present-day glaciers in Austria are limited to the highest ranges in the western part of the country. The investigated glaciated mountain ranges are labelled (Map B). Map C locates the glaciers within the Glockner range that have been used for model validation using geophysical field data

2009. Glacier extents are taken from the Austrian glacier inventories (GI) (Fischer et al., 2015b). More information on the data used is provided below.

The model GlapTop2 (Frey et al., 2014) quantifies ice thickness h based on the shallow ice approximation:

$$h = \frac{\tau}{f \rho g \sin \alpha} \quad (\text{i})$$

where τ is the basal shear stress, f is a shape factor that parameterises apparent lateral drag of U-shaped glacier troughs (Nye, 1965), ρ is the density of ice, g is gravitational acceleration and α is glacier surface slope. Following the approach by Linsbauer et al. (2012), this model utilises an empirical relationship determined by Haeberli and Hölzle (1995) to quantify τ in equation i. Ice thickness is calculated for random points on the glacier surface. α is averaged within a moving window around the random cell. The moving window is scaled to meet a minimum elevation range to avoid very low slopes, which would lead to unrealistically thick ice in (i). Ice thickness at the random points is finally interpolated to the entire glacier surface. Ice thickness at glacier margin cells is set by the user. We reproduced the model in a Python script, which allowed the modification of model parameters for testing.

A uniform shear stress τ is obtained for each glacier based on the formula by Haeberli and Hölzle (1995):

$$\tau [\text{kPa}] = 0.5 + 159.8 \Delta H - 43.5 (\Delta H)^2 \quad (\text{ii})$$

for glaciers with $\Delta H < 1.6$ km, where ΔH is the elevation difference along the entire glacier. For glaciers with $\Delta H > 1.6$ km ($n = 1$ in GI1, 0 in GI3), a τ of 150 [kPa] is applied (Frey et al., 2014). Consequently, the only remaining variable on the right side of (i) is surface slope α , which determines the shape of the bedrock topography, while τ scales with elevation for each individual glacier.

For comparison, we also applied the approach of Huss and Farinotti (2012) for ice thickness modelling (HF model). The HF model was developed from the ice thickness estimation method presented by Farinotti and others (2009). The HF model scored highest among the automated methods applicable at large scales compared within the Ice Thickness Models Intercomparison eXperiment (ITMIX; Farinotti et al., 2017), and has already been applied to all glaciers globally (Huss & Farinotti, 2012) and for regional glacier volume studies (e.g. Andreassen et al., 2015; Frey et al., 2014).

The basic principle of the HF model is the estimation of ice volume flux along the glacier, from which local ice thickness is computed based on measured surface slope and the flow law for ice. The approach accounts for basal sliding conditions, variations in the valley shape, and the influence of ice temperature on ice flow using several adjustable parameters. The surface mass balance and the volumetric balance flux are calculated along a simplified longitudinal profile of the glacier flow line for estimating the mean ice thickness of individual elevation bands. In a final step, ice thicknesses are extrapolated from the flow line to all cells within the glacier extent on a regular grid considering local surface slope and distance from the glacier margin. We refer to Huss and Farinotti (2012) for more details on the model architecture. We ran the model for 10 m elevation bands. Valley shape

factor, continentality and climate parameters were kept as proposed in Huss and Farinotti (2012).

Both models were calibrated using low-resolution ice thickness measurements from 58 glaciers in the Austrian Alps (Fischer et al., 2015). The calibration procedure was developed by Helfricht et al. (2019) for the HF model and adopted to calibrate the GlapTop2 model used in this study. Measured ice thickness data have been homogenised due to temporal offsets between field surveys and our modelling periods. The time of ice thickness measurements ranges between 1995 and 2010. Field data were first homogenised to the date of an intermediate glacier inventory (GI2), based on topographic surveys from 1996 to 2002. This was chosen by Helfricht et al. (2019) because they also modelled the ice thickness for GI2, and because it was closest to the time of field surveys. First, the mean annual ice thickness change between GI2 and GI3 was quantified from glacier surface elevation change (z). For the calculation of GI2 ice thickness (h_{GI2}), the mean annual thickness change between GI2 and GI3 was multiplied by the number of years (y) between GI2 and the time of field measurement and added to the measured ice thickness (h_M).

$$h_{GI2} = h_M + \left(\frac{z_{GI3} - z_{GI2}}{Y_{GI3} - Y_{GI2}} \right) * (Y_M - Y_{GI2}) \quad (\text{iii})$$

The ice thickness (h) in GI1 and GI3 was derived using the observed surface change between the respective glacier inventory and GI2 using:

$$h_{GI1} = h_{GI2} - (z_{GI2} - z_{GI1}) \quad (\text{iv})$$

$$h_{GI3} = h_{GI2} + (z_{GI3} - z_{GI2}) \quad (\text{v})$$

Helfricht et al. (2019) report an overall uncertainty of this approach of 11% for GI1 and 13% for GI3. For more information on the ice thickness homogenisation, refer to Helfricht et al. (2019).

These adjusted ice thickness measurements were used for parameter testing and calibration of both models. For GlapTop2, we applied a similar procedure as Frey et al. (2014) by testing different values for the shape factor ($f, \pm 0.1$), the applied shear stress ($\tau, \pm 20\%$) and the interpolation method (Inverse Distance Weighted and TopoToRaster; Hutchinson, 1989). These modified model parameters simulate different shapes and dimensions of glaciers targeting to approach the nature of glaciers in our study area (Table 1). For the HF model, Helfricht et al. (2019) altered the apparent mass balance gradient for calibration (see their publication for more details). Calibration of both models was done using 3,500 (GI1) and 3,200 (GI3) point measurements of ice thickness at 58 glaciers (Fischer et al., 2015) and for each glacier inventory with the effort to reduce the mean absolute error (MAE) between modelled and measured ice thickness. For GlapTop2, the parameter combination with the lowest MAE was used for modelling of GBOs (Table 1).

Furthermore, we also produced a bulk averaged model ice thickness for each time period (GI1_av, GI3_av) by generating a mean ice thickness of both GlapTop2 and HF. This is based on the experiences of the ITMIX study by Farinotti et al. (2017) and on Farinotti et al. (2019), who conclude that a combination of different models leads to improved modelled ice thickness.

TABLE 1 Model runs with modified model parameters used for calibration of GlapTop2

Model run	Shape factor (<i>f</i>)	Maximum shear stress (τ , kPa)	Interpolation method
Var1	0.8	150	IDW
Var1m	0.8	120	IDW
Var1p	0.8	180	IDW
Var2	0.8	150	TTR
Var3	0.7	150	IDW
Var3m	0.7	120	IDW
Var3p	0.7	180	IDW
Var4	0.9	150	IDW
Var4m	0.9	120	IDW
Var4p	0.9	180	IDW

To derive GBOs, we applied a fill-sinks algorithm to the modelled subglacial topography and extracted the filled locations following Linsbauer et al. (2012). We considered modelled depression $> 10,000 \text{ m}^2$ in accordance with previous studies (Frey et al., 2014; Linsbauer et al., 2012; Linsbauer et al., 2016). Finally, to assess the GBOs with the greatest confidence of prediction, we analysed the ensemble of all model runs (GlapTop2 in GI1 and GI3, HF model in GI1 and GI3, GI1_av, GI3_av) within the boundaries of the 2015 glacier extent. We intersected all model run results and generated a raster data set containing the number of intersecting models within the simulated GBO area. We assigned the greatest confidence to areas where all six model runs predict a GBO and lower levels of confidence at zones with a lower number of model predictions accordingly. Objects resulting from this intersection have been filtered to areas $> 10,000 \text{ m}^2$.

3.2 | Data for modelling and evaluation

Both models require two kinds of input data: (1) glacier outlines, and (2) a digital elevation model (DEM) of the ice surface at the same period. In Austria, several data sets on glacier outlines exist, resulting in different glacier inventories (GI). Outlines representing glacier extents from 1850 (GI LIA), 1969 (GI1), 1996–2002 (GI2), 2004–2012 (GI3) and 2015 (GI4) are available. The glacier outlines were mapped manually using orthophotos and airborne laserscan data with varying acquisition dates (Buckel & Otto, 2018; Fischer et al., 2015a; Patzelt, 2013). We used data from GI1 and GI3, representing the dates 1969 and around 2009, respectively, because for these periods digital elevation data are available, which are required for modelling (Fischer et al., 2015b). Additionally, we applied the GI4 extent to assess GBOs that have not been exposed by glacier melt yet. GI1 data are based on aerial images from 1969, while glacier extents in GI3 were mapped on both orthophotos and illuminated airborne laserscan (ALS) data between 2004 and 2012, with most glaciers mapped in 2009 (Abermann et al., 2009; Fischer et al., 2015b). GI4 data are based on orthophoto mapping (Buckel et al., 2018). We used different DEMs for the two modelling periods. At GI1, we applied a DEM with 10 m resolution derived from aerial photographs with a vertical accuracy of $\pm 1.9 \text{ m}$ (Lambrecht & Kuhn, 2007). For the GI3 period, we used a 10 m DEM based on ALS data from 2006 to 2012 provided by Open Data Österreich, with a vertical accuracy of 0.15 m ([\[gv.at\]\(http://data.gv.at\)\). We applied both models to glaciers with an area \$> 100,000 \text{ m}^2\$ at GI1 and analysed a total of 616 glaciers with a size of \$529 \text{ km}^2\$ at GI1. Total glacier area decreased to \$397 \text{ km}^2\$ at GI3 and less than \$320 \text{ km}^2\$ at GI4.](http://data.</p>
</div>
<div data-bbox=)

We evaluate the model performance in several ways. First, ice thickness models are compared with the global consensus data on glacier ice thickness by Farinotti et al. (2019). The data set covers 525 of the 616 glaciers studied. The Farinotti et al. (2019) data set uses glacier outlines of the RGI 6.0 (Randolph Glacier Inventory), which was published in 2017. RGI 6.0 glaciers for the Austrian Alps are slightly smaller than glaciers at GI3. For large glaciers ($> 50,000 \text{ m}^2$), outlines correspond well with the other inventories. Smaller glaciers are often misrepresented, probably owing to the different data acquisition technique. The RGI data were derived automatically from LANDSAT TM imagery (Pfeffer et al., 2014; RGI Consortium, 2017) in contrast to manual mapping on high-resolution orthoimages for the Austrian Glacier inventories.

Second, modelled GBOs were compared with existing glacial lakes listed in the Austrian lake inventory (Buckel & Otto, 2018). Number, location and size of the modelled GBOs from the GI1 and GI3 model runs were compared with lakes, which evolved between GI1 and GI4 because of ice retreat. This comparison faces some restrictions due to the nature of the modelling approach that only delivers bedrock-dammed lakes. Therefore, only lakes classified as *bedrock-dammed* and *embedded-in-glacial-sediment* were considered for this comparison (see Buckel et al., 2018 for details on classification). The latter type is chosen, assuming that it represents locations where bedrock depressions have been partially covered with debris, masking the bedrock dam. In this step, we first selected both lakes and GBOs within the area released by glaciers between GI1 and GI3 and GI3 and GI4, respectively. Subsequently, lakes and GBOs of the respective model runs were intersected on an object basis.

Third, modelled ice thickness and bedrock locations were compared with field data derived from high-resolution geophysical surveys of individual glaciers. A crucial control on the quality and resolution of ground-penetrating radar (GPR) data is the choice of antenna frequency, the density of measurements and the accurate positioning on the glacier. Very low frequencies and large measurement intervals may result in low-resolution and low-accuracy images of the bedrock interface. The ice thickness data by Fischer et al. (2015) used for model calibration was derived using a low-frequency antenna (3–6 MHz). Most of these data were collected using a very large

measurement spacing of 100 m and more. Consequently, the bedrock topography may not be represented well enough to identify bedrock depressions using these data. Further, the data set by Fischer et al. (2015) does not include information on glacier surface height at the time of data acquisition. Thus, it cannot be used to determine the topography of the glacier bed and compare potential bedrock depression locations.

We used high-resolution GPR data collected at three typical cirque glaciers, Schmiedingerkees, Wurtenkees, and Goldbergkees glaciers, as well as reflection seismic data collected at the Pasterzenkees glacier (refer to Figure 1 for locations). Modelling results are evaluated along linear sections using interpolated bedrock surfaces based on the geophysical data. Additionally, we detected GBOs also within the interpolated bedrock surface following the same procedure as for the modelled surfaces. Reflection seismic data were collected in 2009 (Binder et al., 2011). GPR data on Schmiedingerkees were collected in 2016 (unpublished data), and data on Wurtenkees (Binder, 2009) and Goldbergkees were collected between 2002 and 2004 (Binder et al., 2009). GPR data sets have been collected using antenna frequencies of 100 MHz for Schmiedingerkees and 20 MHz for the other glaciers (Binder et al., 2009). GPR data sets have been collected pointwise with a common-offset acquisition geometry and intervals of 1 m (Schmiedingerkees) and 2 m (Wurtenkees, Goldbergkees). GPR traces were positioned with Differential Global Positioning System (DGPS). A standard signal processing was applied on the GPR data. Migration images correctly sloped undulating reflectors, which makes it an essential processing step for U-shaped subsurfaces like glacial bedrocks (Binder et al., 2011). A standard 2D migration was applied for the Schmiedingerkees data set, and a 3D migration routine was applied for the Pasterzenkees, Wurtenkees and Goldbergkees data sets (further described in Binder et al., 2009). Bedrock features have been picked manually on filtered and migrated radargrams. For the Schmiedingerkees, 1,550 individual bedrock points have been picked. For Wurtenkees and Goldbergkees, 2,800 and 2,030 points have been picked representing bedrock topography (Binder et al., 2009). The GPR data at the Schmiedingerkees were interpolated using the TopoToRaster tool in ArcGIS (Hutchinson, 1989). The GPR data of Wurtenkees and Goldbergkees were interpolated following a glacier mechanical approach with the assumption of minimum spatial variation of the basal shear stress (Binder et al., 2009). The GPR and seismic data sets of the Pasterzenkees were jointly processed and interpolated following Binder et al. (2009); details are described in Binder et al. (2011). For the Pasterzenkees, reflection seismic data have been jointly migrated and interpolated in combination with low-frequency GPR data by Span et al. (2005).

4 | RESULTS

4.1 | Calibration and comparison of ice thickness models

Both models have been calibrated using GPR-based ice thickness values from more than 50 glaciers in the study area. For GlapTop2, a mean absolute error (MAE) between 29 and 56 m was reached by the various model runs compared with the reference data (Table 2A). For GI1, lowest MAE was established using parameter set *Var1m* (refer to

Table 1 for parameter details). For the GI3 extent, *Var1m* is slightly outperformed by *Var4m*. These two parameter sets have been used for the simulation of GBOs consequently. Calibration of the HF model by Helfricht et al. (2019) generated significant lower MAE values compared to GlapTop2 (Table 2B). The MAE of the consensus data presented by Farinotti et al. (2019) is in the same range as GlapTop2 (Table 2C).

We investigated 616 glaciers with a size of >100,000 m² at GI1. More than 90% of the glaciers investigated can be classified as mountain glaciers at GI1, mostly cirques and niches, characterised by glacier termini that did not reach the valley floors, (Table 3). Glacier melt increased this proportion to 95% at GI3. A total volume of 18.8 and 24.4 km³ of ice at GI1 was modelled by GlapTop2 and HF, respectively. Total volume decreased to 11.5 (GlapTop2) and 16.1 km³ (HF). The data set published by Farinotti et al. (2019) simulates a total volume of 18.7 km³ for 505 of the 616 glaciers analysed in this study (Table 3). Figure 2 visualises the derived subglacial topography based on these thickness models along a profile section on the Pasterzenkees in comparison with the GPR data by Fischer et al. (2015) and an interpolated bedrock model generated from seismic and GPR data by Binder et al. (2011). Significant differences are apparent in the bedrock location upslope and downslope of the ice fall. At the plateau-like upper part of the glacier, all models deviate from the geophysical data, overestimating the depth of the bedrock. The Farinotti et al. (2019) data set has the largest offset to the geophysically derived bedrock with deviations of up to 100 m, while GlapTop2 and HF deviate by 40–50 m. The ice fall area is well represented by all models. In the tongue area, bedrock surfaces become very similar with increasing distance from the ice fall. Between 4,500 and 6,500 m, all models generate a highly similar bedrock surface with deviations well below 30 m that corresponds well to the seismic data.

4.2 | Locations and characteristics of GBO modelled at two different periods

We simulated GBOs at two glacial stages, 1969 (GI1) and 2009 (GI3), using ice thickness modelled by GlapTop2 and HF as well as an averaged ice thickness of the two models for each time period. Between 127 and 305 GBOs are simulated within the different glacier extents, covering a total area between 5.9 and 12.7 km² (Table 4). While the total area of GBOs per time period is similar between the models, the HF model generates more GBOs and GBOs of smaller mean size compared with GlapTop2. Using the averaged ice thickness data generates a similar number of lakes compared with GlapTop2, but the GBOs are of smaller mean size and sum up to a smaller total area. GlapTop2 generates deeper GBOs compared with the other models, which sum up to a maximum total volume of 0.21 km³ for GI1. The total volume and depth of the averaged ice thickness models (GI1_av, GI3_av) are significantly reduced compared with the other models. Compared with GI1, the number of GBOs simulated for GI3 decreases by 30–40%, while the total area and volume of the simulated GBOs decreases by 45% and 50%, respectively.

Frequently, we observed good agreement in the spatial distribution of the GBOs between the model runs as exemplified in the Großglockner area (Figure 3a). Here, depressions modelled by GlapTop2 (purple colours) are often larger, compared with several

TABLE 2 Mean absolute error (MAE) between modelled and measured ice thickness. (A) MAE quantified for different parameter variations in GlabTop2. The underlined values indicate the parameter set used for the final modelling of GBOs. (B) MAE for HF model derived by Helfricht et al. (2019). (C) MAE between measured and modelled thickness in direct comparison with data by Farinotti et al. (2019) for GI3 (note: number of reference points is smaller compared with (A) and (B) owing to smaller number of glaciers provided by Farinotti et al. (2019))

A)		MAE (m) of model test runs GlapTop2								
Inventory	Var1	<u>Var1m</u>	Var1p	Var2	Var3	Var3m	Var3p	Var4	<u>Var4m</u>	Var4p
GI1	34.3	<u>31.0</u>	44.2	34.9	41.0	32.0	55.9	31.9	32.2	37.4
GI3	33.8	29.1	43.7	35.0	40.3	31.0	53.9	30.3	<u>29.0</u>	36.4
B)		MAE (m) of HF model								
GI1	23.0									
GI3	20.1									
C)		MAE (m) of models within glaciers of RGI 6.0								
	GlabTop2	HF	Farinotti et al. (2019)							
GI3	26.6	23.5	29.8							

TABLE 3 Characteristics of the glaciers investigated (min. size > 100,000 m² at GI1)

No. of glaciers: 616 (RGI 6.0*: 505)					Glacier type		Modelled volume		
Period	Total area (km ²)	Mean area (m ²)	Min altitude (m)	Mean altitude (m)	No. mountain glaciers	No. valley glaciers	GlabTop2 (km ³)	HF (km ³)	Farinotti et al. (2019)
GI1	529	859,337	1755	2,868	568	49	18.8	24.4	
GI3	397	644,864	1756	2,884	582	37	11.5	16.1	
RGI 6.0	350	649,972	2020	3,421	471	34			18.8

*Randolph Glacier Inventory.

FIGURE 2 Comparing the location of the bedrock topography derived from the three different ice thickness models along a profile section on the Pasterzenkees glaciers. (1) marks the ice fall

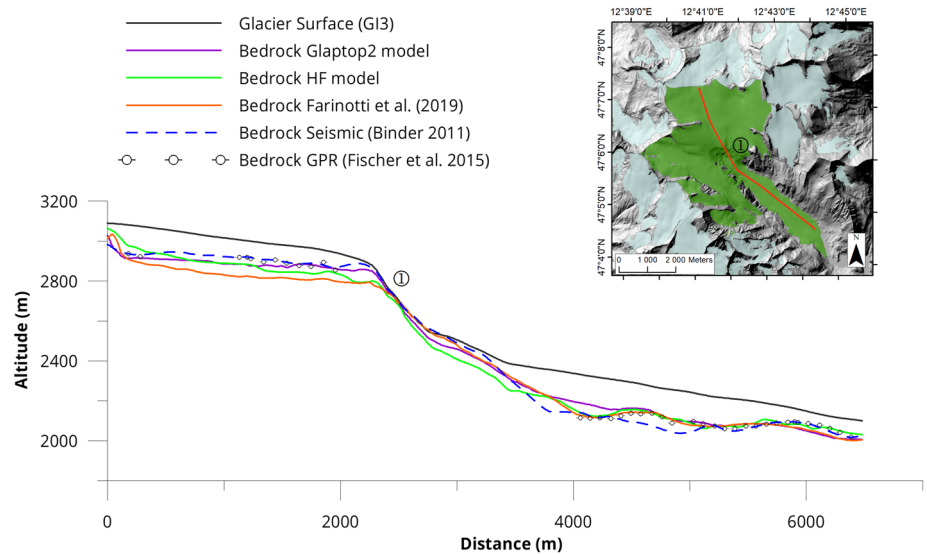


TABLE 4 Number, area, volume and depth of modelled GBOs per model and time period

Modell	Period	Total number	Total area (km ²)	Mean area (m ²)	Total volume (km ³)	Mean depth (m)*	Max. depth (m)*
GLABTOP2	GI1	199	12.7	63,912	0.21	7.4	125
	GI3	141	7.0	50,149	0.10	7.1	90
HF	GI1	305	12.6	41,423	0.16	6.8	110
	GI3	190	7.4	38,948	0.08	6.2	90
GI1_av	GI1	207	10.5	50,649	0.11	5.9	67
GI3_av	GI3	127	5.9	46,715	0.06	5.9	62

*Depths that have been considered modelling artefacts have been omitted.

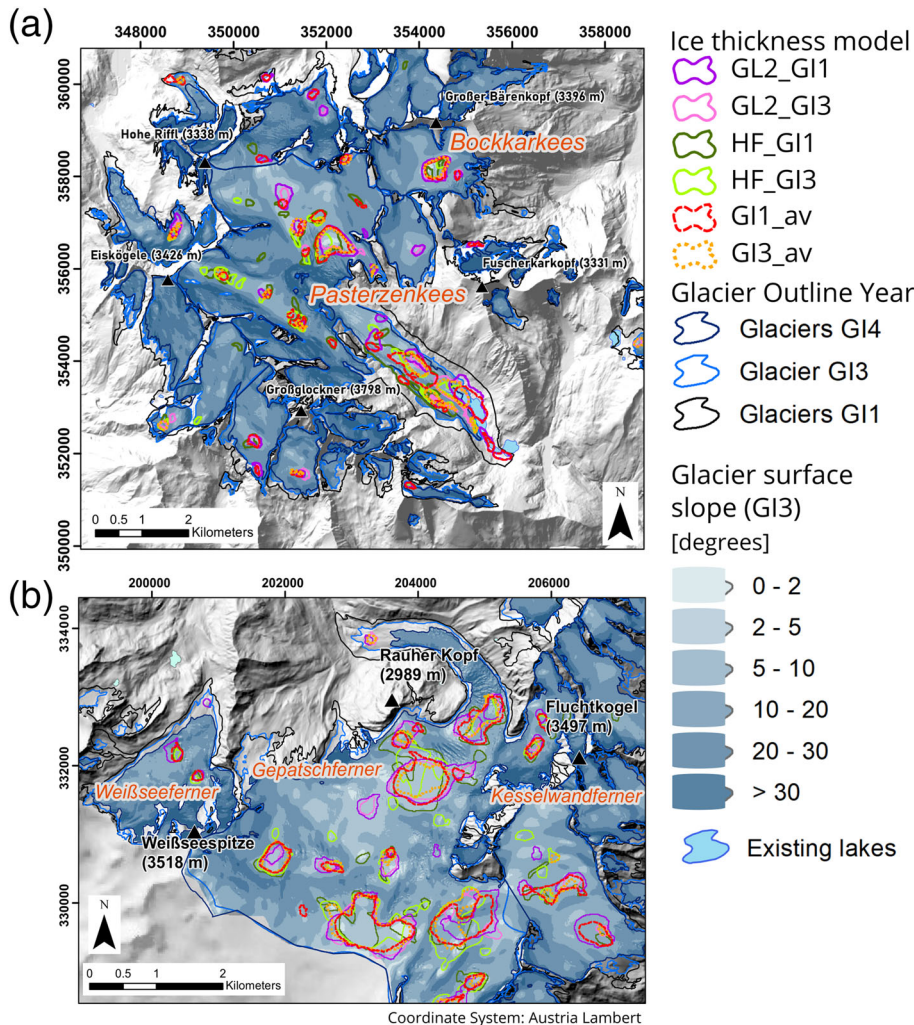


FIGURE 3 Locations of simulated GBOs at the Pasterzenkees area (a), Gepatschferner area (b)

small depressions at the same locations produced by HF (green colours) and the averaged models (dashed lines red (GI1_av) and orange (GI3_av)). In the case of the Pasterzenkees glacier tongue, the results are reversed with larger depressions predicted by the HF model compared with several smaller features derived by GlapTop2 and the averaged models. Even though GBOs generated by the HF model are more abundant and of smaller dimension, the HF model also produced the largest GBOs (Figure 4). More than 50% of all modelled depressions have a surface area smaller than 20,000–26,000 m² (Figure 4a). The largest depression measuring more than 800,000 m² was generated by HF at the Pasterzenkees glacier using the GI1 glacier extend (Figure 3a). The Pasterzenkees is Austria's largest glacier with a characteristic glacier tongue. The tongue area, contains the country's largest proglacial lake that evolved since 2004 (Avian et al., 2020). In the 1990s, fossil peat was discovered at the Pasterzenkees, dated to around 7,500 a/BP, indicating that at this location lakes also existed in the past (Nicolussi & Patzelt, 2000; Slupetzky, 1993). All simulations produce exceptionally large GBOs with surface areas of >500,000 m² mainly at three locations within the Gepatschferner glacier, Ötztal Alps (Figure 3b). GlapTop2 shows the highest agreement in GBO position between GI3 and GI1. Eighty percent of the GBOs simulated at GI3 have also been simulated using the GI1 DEM. This agreement is smaller for the averaged ice thickness models (76%) and drops to 66% for the HF model.

The simulated GBOs have mean depths between 5.9 and 7.4 m, with 50% of the depressions below 6 m (Table 4). Around 80% of the modelled GBOs have a mean depth < 10 m for all models and times. Maximum depths of GBOs reach values between 40 and 125 m. These are located at very flat glacier zones with inclination < 5°. The largest volumes have been simulated for both periods at the plateau like accumulation zone of Gepatschferner and within the Pasterzenkees tongue, the two largest glaciers of the study. Maximum volumes of >25 × 10⁶ m³ have been simulated by GlapTop2 (both GI1 and GI3) at the Gepatschferner and >20 × 10⁶ m³ by HF (GI1) at the Pasterzenkees. GBOs detected within the averaged ice thickness data do not exceed 13 × 10⁶ m³ in GI1 and GI3.

4.3 | Model evaluation using existing lakes

We compared our modelling results from the two different periods with mapped lakes in the study area. In the proglacial area between glacier extents of GI1 and GI3 (period 1) and between GI3 and GI4 (period 2), 82 and 61 lakes have been mapped, respectively (Table 5), with 21–30% of the existing lakes being represented by the simulated GBOs (right positive). The models are not capable to predict between 70% and 79% of mapped lakes (false negative). Between 50% and 72% of the GBOs have been modelled at locations where no lake was

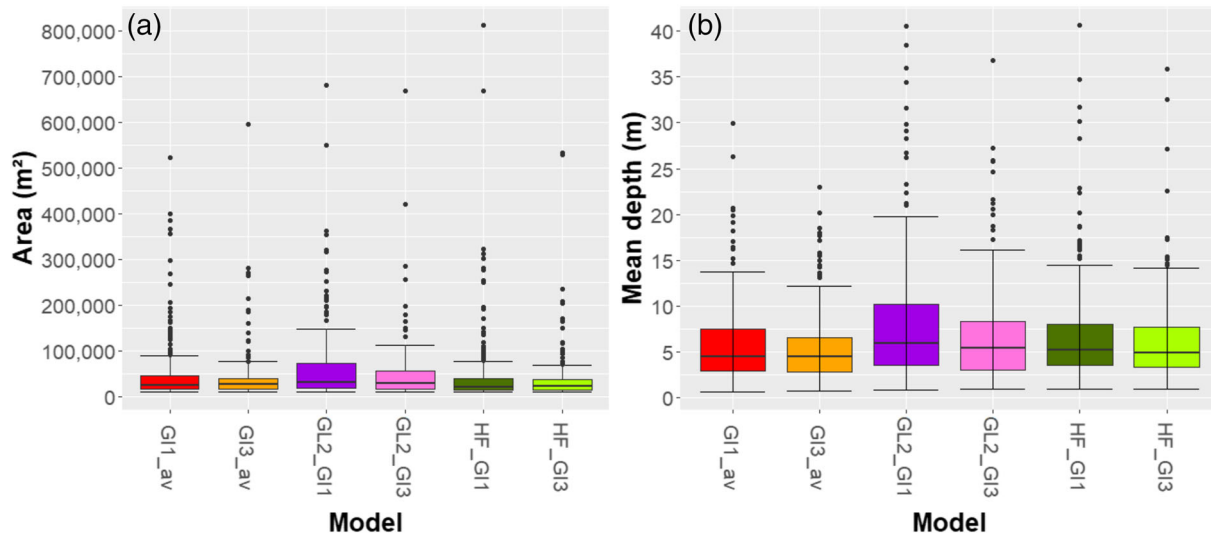


FIGURE 4 Distribution of area (a) and depth (b) of simulated GBOs

TABLE 5 Comparing modelled GBOs with mapped lakes that evolved between 1969 and 2009 and between 2009 and 2015. True positive: modelled GBO matches existing lake. False positive: GBO modelled, but no lake. False negative: existing lake, but no modelled GBO

Period 1: 1969–2009 (GI1–GI3)		Lakes: 82		
Model	No. of GBOs	True positive (no. [%])	False positive (no. [%])	False negative (no. [%])
GlacTop2	34	17 (21%)	17 (50%)	65 (79%)
HF	76	25 (30%)	51 (67%)	57 (80%)
GI1_av	52	19 (23%)	33 (63%)	63 (77%)
Farinotti et al. (2019)	64	10 (12%)	54 (66%)	72 (88%)
Period 2: 2009–2015 (GI3–GI5)		Lakes: 61		
Model	No. of GBOs:	True positive (no. [%])	False positive (no. [%])	False negative (no. [%])
GlacTop2	47	13 (21%)	34 (72%)	48 (79%)
HF	47	15 (25%)	32 (68%)	46 (75%)
GI1_av	40	12 (21%)	28 (68%)	48 (79%)

mapped (false positive). For comparison, using the ice thickness model by Farinotti et al. (2019), only 12% of the lakes evolved between GI1 and GI3 are simulated and 88% of the existing lakes have been missed (note that the number of glaciers in the data set is smaller compared with the other models; see chapter 3.1). Figure 5 illustrates the model performance in relation to existing lakes in the Großvenediger range. While the proglacial lakes in the Obersulzbachkees glacier forefield (orange circles) are reproduced by all models, the lake in the neighbouring Krimmler valley (red circle) is not predicted by any of the models. One reason for this missing GBO is that lake formation started before GI1, suggesting that parts of the lake were already present in the DEM used for modelling GI1 depressions. This shows that the simulation of GBOs that are only partially covered by the glacier at the modelling time is difficult. In this case, the glacier tongue most probably retreated largely from the flat area, thus preventing the generation of a GBO by the models. The example of Obersulzbachkees glacier also shows that, though the models predict the general locations of the existing lakes correctly, shape and size between the modelling result and the real lakes differ in most cases. Lake Obersulzbach, for example (Figure 5), evolved between 1999 and 2012 and has a size of about 180,000 m² and a volume of 2.5 × 10⁶ m³ (derived from unpublished lake bathymetry surveys). The

geometry of the lake is best reproduced by GlacTop2 at GI1, which simulated a GBO of 170,000 m² with a volume of 2.7 × 10⁶ m³. In contrast, the HF model (GI1) generates a GBO of 28,000 m² with a volume of 170,000 m³. The same is true for the lake evolved at the Pasterzenkees (Figure 3a), where the models generate GBOs of various characteristics and locations within the glacier tongue. The existing lake, however, formed at a location at the frontal part of the GI 1 glacier extent that is only marginally covered by the HF depressions and slightly better represented by GlacTop2 (Figure 3).

4.4 | Comparing modelling results with measured ice thickness data from geophysical surveys

We compared the modelling results with high-resolution geophysical data that detected the subglacial topography at three typical cirque glaciers and one valley glacier in the study site (see Supplementary Data for additional figures). The geophysical data have been used to interpolate the subglacial topography of the selected glaciers. Modelling results are evaluated along linear sections and by detecting GBOs within the interpolated bedrock topography based on the geophysical surveys. The representation of the bedrock topography by the models

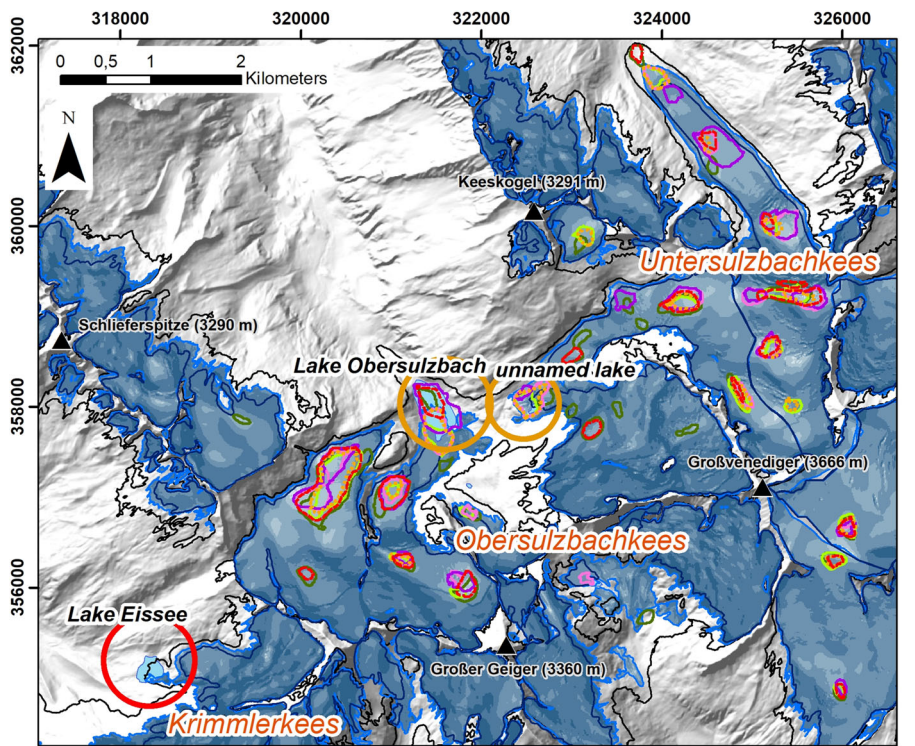
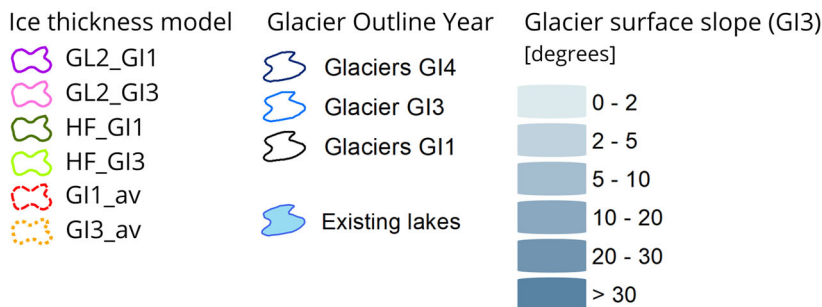


FIGURE 5 Comparing mapped lakes and simulated lakes from the Großvenediger area, Hohe Tauern range. Lakes that are represented by GBOs are marked by the orange circles. Lake Eissee (red circle) is not simulated by any model



is significantly different between profile sections along the flowline and cross-sections (Figure 6, and supplementary figures). At profile sections, simulated bedrock topography often resembles the glacier surface and not the bedrock derived from geophysical surveys. At cross-sections, bedrock topography is much better reproduced by the models, based on visual inspection. At Pasterzenkees (Figure 6) and at Schmiedingerkees (see Supplementary Figure 1), for example, all modelled bedrock surfaces run parallel to the glacier surface and fail to reproduce the curved shape of the geophysically derived bedrock when compared along profile sections. In contrast, along cross-sections, the trough shape of the bedrock surface is well reproduced at the Pasterzenkees (Figure 6), Wurtenkees (Supplementary Figure 2) and Goldbergkees glaciers (Supplementary Figure 3). However, some models do not match the exact position of the bedrock in cross-sections. The offset between modelled and geophysically derived bedrock is between >20 m and <100 m. GlapTop2 and HF most often generate a similar shape of the bedrock, but frequently HF simulates the bedrock at larger depth compared with GlapTop2. We also observed that the bedrock topography was better reproduced using GI3 DEM data for modelling. Models applying GI1 DEM data tend to produce a bedrock topography at higher distance above the geophysically derived location, thus underestimating the ice thickness. Using the Farinotti et al. (2019) data set, a bedrock topography is generated that is comparable to the other models at the Pasterzenkees (Figure 6)

and Schmiedingerkees (Supplementary Figure 1), but strongly offset at the Goldbergkees and Wurtenkees glaciers with positions far above the measured bedrock (Supplementary Figures 2 and 3). In the later examples, also the shape of the simulated bedrock is completely out of range.

We applied the same GBO detection procedure to the geophysically derived bedrock surfaces to compare the simulated GBOs with the field data. We observed GBOs in the subglacial topography of the Pasterzenkees and the Goldbergkees glacier. At the Pasterzenkees glacier, 13 GBOs can be detected within the subglacial topography derived from geophysical surveys (Figure 7a). Three of them cover areas $>100,000$ m² (Table 6). Two large GBOs are located within the glacier tongue area, while one large GBO is apparent north of the ice-fall within the plateau-like upper zone of the glacier. The southernmost GBO is in contact with the existing proglacial lake, indicating that this lake will continue to expand in the near future. The models simulate between 7 (GlapTop2 GI3) and 21 (HF GI1) GBOs within the Pasterzenkees glacier (Figure 7a). Between six and ten of these GBOs overlap with the GBOs derived from the geophysical data; however, sometimes the simulated GBOs are much smaller compared with the existing bedrock depression (Figure 7a). The GBOs derived from geophysical surveys have a total volume of 27.8×10^6 m³, of which more than 95% are covered by the three largest GBOs. These are reproduced with different dimensions by the simulations (Figure 7a,

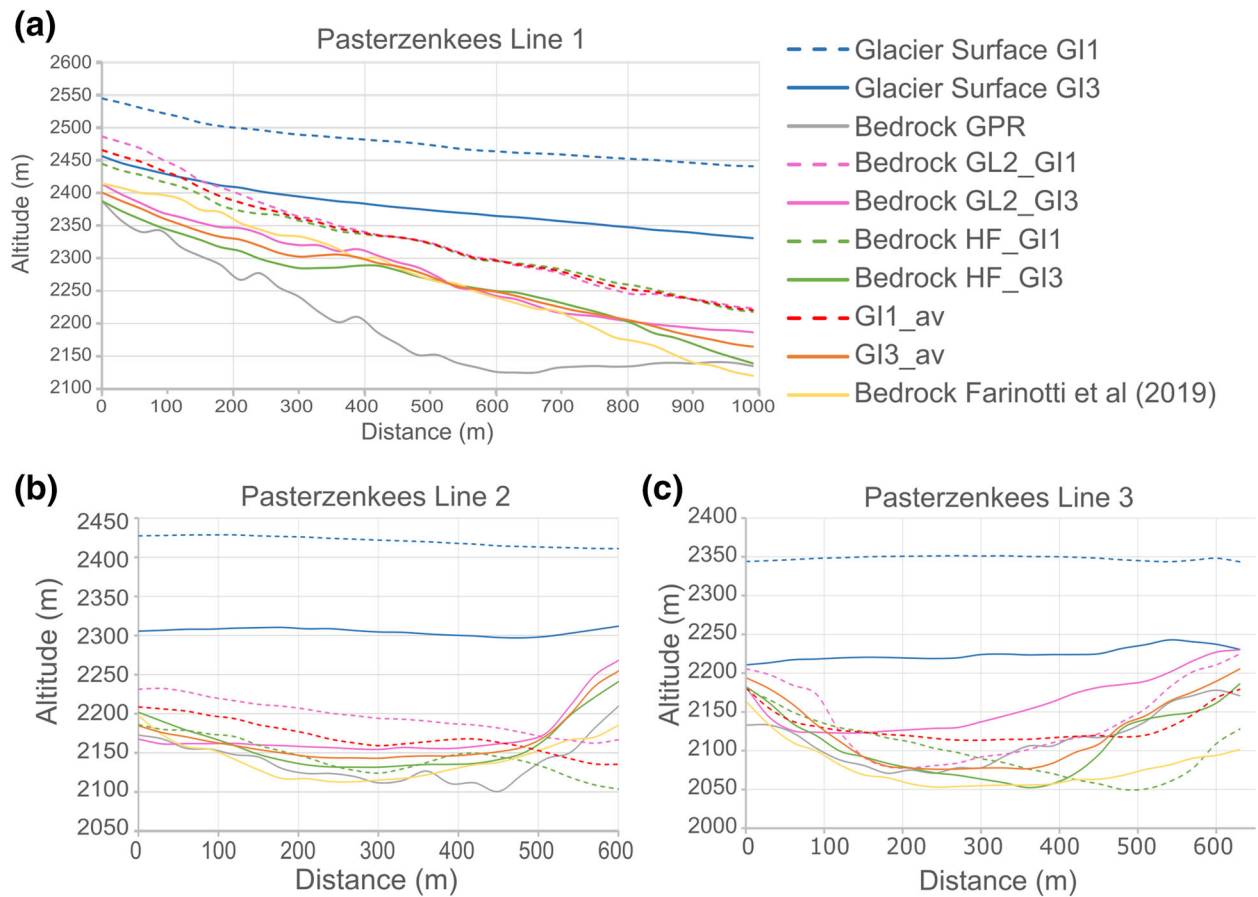


FIGURE 6 Location of measured and modelled glacier beds at the Pasterzenkees glacier tongue. Refer to Figure 1 C for location of the glacier and to Figure 7 for location of the profile lines

Table 6). At the plateau-like upper zone (GBO 1), all models produced depression of similar size, but varying volumes. Except for HF GI1, all models generate smaller volumes compared with the reference data. The two GBOs located in the tongue area are simulated with highly differing areas and volumes, with none of them coming close to the volumes found within the geophysical data. At the same time, the entire tongue area contains several modelled GBOs of various size, which are not observed in the reference data.

At the Goldbergkees, three GBOs are apparent in the GPR data, one in the upper and central part, one at a marginal position in the centre and one towards the glacier tongue (Figure 7b). The latter GBO corresponds well to a proglacial lake that has evolved at the glacier tongue since 2015. Another, ice-marginal lake has formed recently at the upper end of the glacier, which is located within the largest GBO derived from GPR data and was simulated by all model runs. Only HF at GI3 reproduced GBOs at the other locations, however, with much smaller extent. The lake and GBO (from geophysics) in the frontal part of the glacier could not be reproduced by the applied models. The measured GBOs have a total volume of $6.6 \times 10^6 \text{ m}^3$ with a maximum depth of 67 m at the largest GBO apparent in the GPR data (Figure 7b). The simulations generate much smaller volumes and depths, and the maximum depth of these depressions is shifted 350 m uphill of the measured location.

4.5 | Assessing the potential locations of future lakes in Austria

The application of six different ice thickness models enables us to use the ensemble of simulated GBOs for a confidence estimation of potential locations where future glacier lakes may evolve despite other sources of uncertainties such as sedimentation or drainage. We consider locations where five or more models predict a GBO as high confidence, which is the case at 42 locations for predicted GBOs $> 10,000 \text{ m}^2$ (Table 7). The total area of potential new lakes sums up to around 2 km^2 . These locations are within the boundaries of 23 glaciers, most of them in the Ötztaler Alps, the Venediger Range and the Glockner Range (Figure 8). Especially within the largest glaciers Pasterzenkees and Gepatschferner, several new glacial lakes may evolve (Figure 8b,c). Most potential future lakes are simulated in mid-to-up-glacier locations, with very few being located close to the lower glacier margin. About 30% of these potential future lakes are located within a distance of $< 500 \text{ m}$ from ridges or steep bedrock slopes. At Gepatschferner, some of the locations are in close vicinity to each other and may result in a single lake (Figure 8b). At the Obersulzbachkees, which has split into several single glaciers in the recent past, three to four new lakes may evolve in addition to the existing two lakes that formed within the last 20 years (Figure 8d).

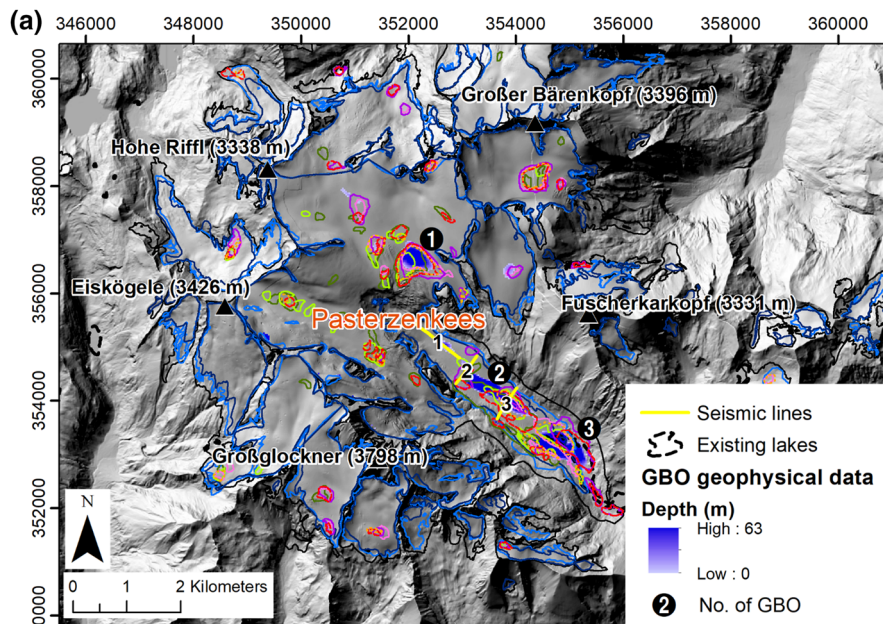


FIGURE 7 Detected GBOs (blue shades) within the interpolated bedrock surface derived from high-resolution geophysical surveys, compared with the modelling results for Pasterzenkees (a) and Goldbergkees (b). White numbers in (a) indicate simulated GBOs discussed in the text. Numbered yellow lines show locations of seismic profiles depicted in Figure 6

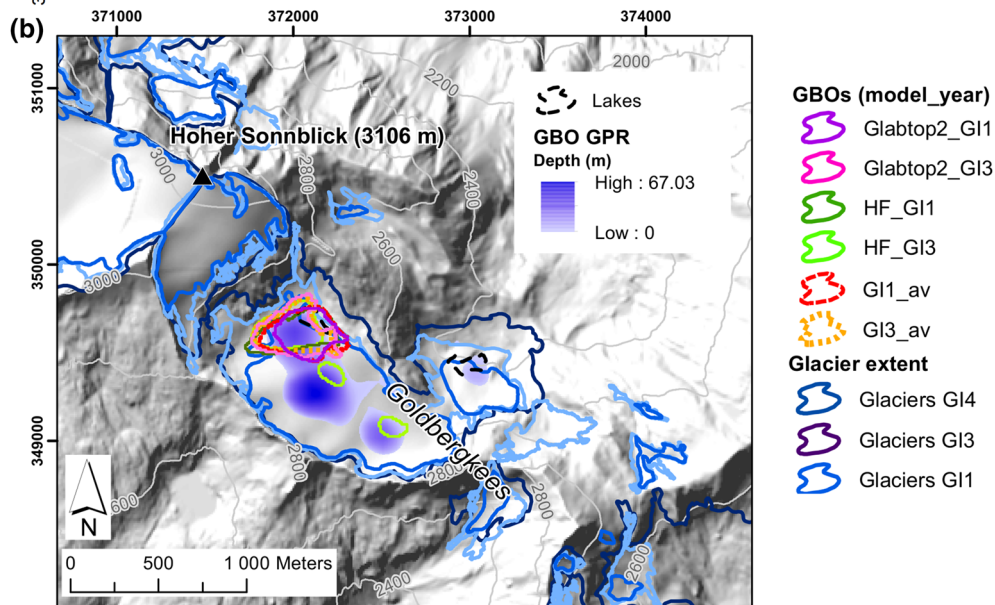


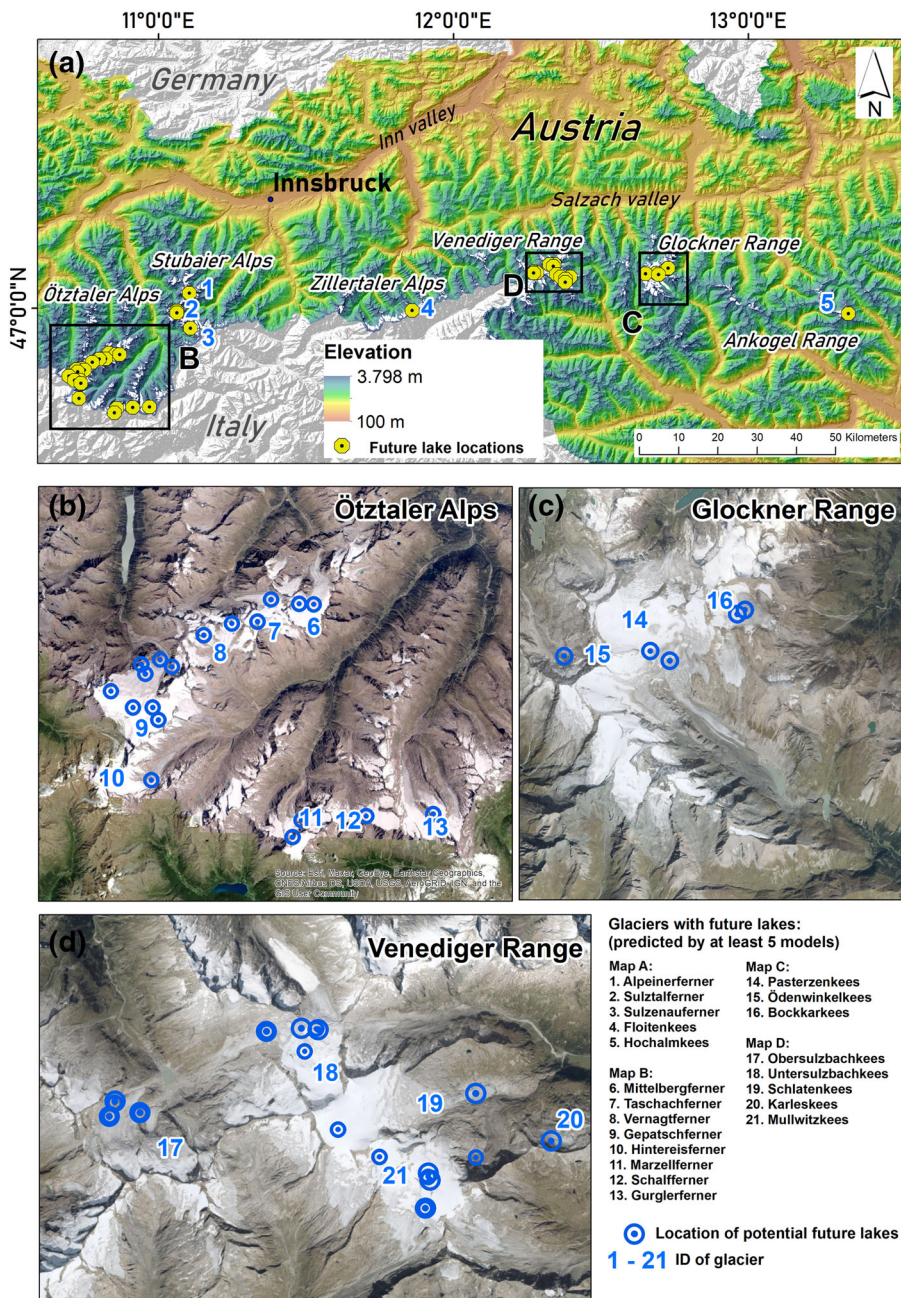
TABLE 6 Geometrical characteristics of the largest GBOs located within the Pasterzenkees compared with the modelled GBOs at these locations

Geophysical data				GL2 GI1	GL2 GI3	HF GI1	HF GI3	GI1_av	GI3_av
GBO no.	Area (m ²)	Depth max (m)	Vol. (m ³)						
1	247,500	45	4,329,000	12,172,791	6,304,519	8,778,960	1,719,120	10,651,100	4,808,920
2	369,900	63	10,475,100	747,670	137,928	22,988,200	4,579,320	3,412,520	1,667,390
3	431,100	57	12,077,100	5,647,792	7,725,501	227,481	1,831,270	3,276,830	4,304,570

TABLE 7 Number of potential future lakes resulting from model intersection

Number of intersecting models	Potential future lakes (cumulative)	Area (km ²)	No. of glaciers with potential future lakes
2 or more	149	9.8	54
3 or more	99	5.6	39
4 or more	61	3.5	28
5 or more	42	2.0	23
6	22	0.8	13

FIGURE 8 Location of simulated GBOs with highest confidence (predicted by a minimum of five models) that are interpreted as potential future lakes in Austria (a). Most of the future lakes will develop within the Ötztaler Alps (b), The Glockner range (c) and the Venediger range (d) (Orthofotos: Basemaps.At,ESRI)



5 | DISCUSSION

5.1 | Number of GBOs and ice thickness estimation

Our modelling approach simulated between 86 and 198 potential GBOs underneath the existing glaciers in the Austrian Alps (GI4, 2015), with a total area between 4.5 and more than 8 km² (Table 8). Since the maximum glacier extent of the Little Ice Age (LIA) in the mid-1850s, 264 lakes evolved that still exist today with a total area of 2.93 km² (Buckel et al., 2018). Considering the remaining glacier area of 330 km², which is only about 30% of the LIA extent, the number and total area of potential GBOs is overestimated significantly. It is obvious that not all potential GBOs will turn into lakes, since sediment deposition within the subglacial topography may fill potential depressions during glacier downwasting. Furthermore, some lakes may drain, or evaporate once the water input from the melting glacier ceases or

water drains into the ground in karst areas (Carrivick & Tweed, 2013; Salerno et al., 2014). On the other hand, for the same reasons, some lakes may have disappeared already since the LIA. However, as previously stressed, the GBO detection approach is restricted to the prediction of potential bedrock-dammed lakes, which account for less than 50% of the existing lakes (Buckel et al., 2018). Nevertheless, this mismatch may also result from insufficient performance of the approach to simulate subglacial topography of the glaciers in Austria. Despite the same reference data for calibration, the HF model generates 40% greater total ice volume compared with GlapTop2. At the same time, the model calibration of HF allowed for a smaller MAE compared with GlapTop2. This was also previously observed by Frey et al. (2014), although their difference between GlapTop2 and HF was significantly smaller. The observed MAE values by both models are comparable to similar studies (e.g. Pelto et al., 2020). In comparison, the Farinotti et al. (2019) data represent a total volume around 60% greater than GlapTop2 and 15% greater than HF, while having the

TABLE 8 Simulated GBOs within the glacier extent at GI4 (2015)

Model	Number	Area (km ²)	Volume (km ³)
GL2 GI1	123	8.7	0.15
GL2 GI3	95	5.3	0.07
HF GI1	198	8.1	0.09
HF GI3	143	6.0	0.07
GI1_av	140	7.8	0.09
GI3_av	86	4.5	0.05

highest MAE when compared with the ice thickness field data. Considering that many small glaciers are poorly represented by the RGI 6.0 data, the overestimation of the larger glaciers within the Farinotti et al. (2019) model is considered substantial. With respect to the GBO simulation, Farinotti et al. (2019) produced the lowest matching with existing lakes (Table 5).

GlacTop2 calibration revealed that for both time periods different parameter sets lead to minimised MAEs. For GI1, a shape factor of 0.8 and a 20% reduced shear stress (τ) was applied. For GI3, the lowest MAE was reached using a shape factor of 0.9 and a 20% reduced shear stress. Parameter testing showed that a reduction of the shape factor to 0.7 as well as an increase in shear stress by 20% lead to an increase in MAE, both factors contributing to generate a larger ice volume compared with other combinations of f and τ . This was previously reported by Frey et al. (2014). A similar parameter testing was also performed by Ramsankaran et al. (2018), who derived a shape factor (f) of 0.66 for modelling of the ice thickness of a large valley glacier in the Himalayas. Based on the results, they conclude that a glacier-specific shape factor would produce best results using GlacTop2. An adjustment of the shape factor has previously been proposed by Li et al. (2012). However, this kind of adjustment is very tedious with respect to the large number of glaciers investigated in this study.

5.2 | Model accuracy and simulated bedrock topography

A comparison with high-resolution geophysical data revealed that the bedrock topography simulated by GlacTop2 and HF does not correspond well to the observed bedrock. The modelling approach tends to smooth the subglacial topography and fails to capture bedrock variation especially in the vicinity of large topographic changes, like bedrock steps. The HF model visually showed a better performance especially along glacier cross-sections. This may be due to the HF modelling approach that calculates the ice thickness along elevation belts. However, the model underestimates the bedrock elevation partly in the upper locations of the glaciers (cf. Figure 2, Supplementary Figures 2 and 3). This could be due to too little cumulated mass required for mass conservation depending on the apparent mass balance gradient. The offset of bedrock topography simulated by GlacTop2 compared with the field data is often greater than for the HF model. Thus, the resulting location and geometry of potential GBOs are considered less reliable compared with HF. Averaging the ice thickness between the two models leads to a further smoothing of the ice thickness values, resulting in a smaller number and generally

less deep GBOs. Therefore, we ascertain that the model performance in generating a realistic subglacial bedrock topography is rather limited and that the detected locations of potential GBOs may include high uncertainties. This is caused by the low accuracy of the ice thickness models and is also affected by the different ways of interpolating the calculated thickness values. The model calibration allowed for a MAE of 20–30 m, which locally can be much higher. The mean lake depth of <10 m indicates that GBO detection using these data may be challenging. However, we observed GBOs simulated by more than one model at the same locations, indicating that, despite lower ice thickness by GlacTop2, smoothing by the averaged models, or different ways of interpolating the data, the approach is still able to generate GBOs at locations in agreement between the models. These overlapping locations have been considered as most probable locations for potential future lakes. Based on our observations, we conclude that the modelling approach is capable of indicating potential GBO locations within existing glaciers. However, we consider large uncertainties in the simulated size and volume for all models applied. This finding is in line with previous studies (Magnin et al., 2020; Viani et al., 2020). We conclude that simulating GBOs with several models and at different time periods is beneficial for the reduction of uncertainties of locations and dimensions and helps to better predict potential future lakes.

5.3 | Glacier characteristics, climate change impacts and GBO modelling

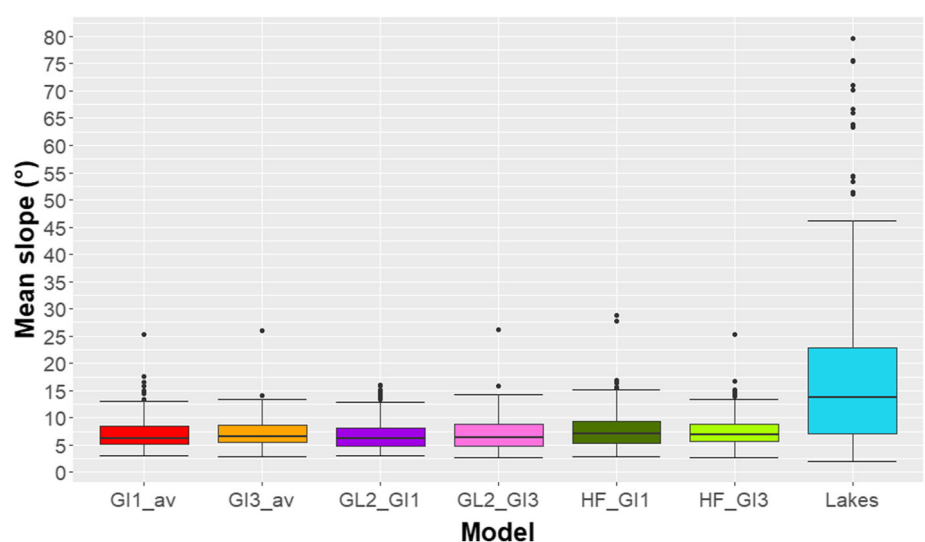
We applied our modelling approach to detect GBOs within a mountain range dominated by mountain glaciers like cirque or niche glaciers. Previous studies focused on regions with much larger glaciers and a greater share of valley type glaciers, like the Himalayas, the Peruvian Andes or the Swiss Alps (Colonia et al., 2017; Frey et al., 2014; Kapitsa et al., 2017; Linsbauer et al., 2016; Pandit & Ramsankaran, 2020). In the Austrian Alps, more than 90% of the glaciers are cirque and niche glaciers and less than 8% of the glaciers can be classified as valley glaciers (Otto et al., 2018). All glaciers suffered significant area and volume loss since the Little Ice Age (Fischer et al., 2015b; Helfricht et al., 2019). Glacier melt led to the disappearance of many glaciers and the retreat of glacier tongues from the valley floors. Consequently, the geometry of many glaciers changed significantly since the Little Ice Age and between the investigated times. Besides changes in glacier length, glacier volume and overall shape, many glaciers disintegrated into single ice bodies. The Goldbergkees, the Wurtenkees and the Obersulzbachkees are typical examples of this behaviour in our study region (Figure 5 and Supplementary Figures 2 and 3). Abermann et al. (2011) showed that glaciers < 0.5 km² in the Austrian Alps decreased more than twice in area between GI1 and GI2 (1998) compared with larger glaciers, indicating a greater climate sensitivity of small mountain type glaciers. With increasing equilibrium line altitudes, climate change alters the mass balance and flow velocities of degrading glaciers (Fischer & Markl, 2008; Stocker-Waldhuber et al., 2019). These changing glacier characteristics can have an impact on the application of the ice thickness models. Originally, the shallow ice approximation was postulated for large ice shields and not for mountain glaciers (Hutter, 1983). The ice thickness models applied in our study contain either assumptions

on the glacier geometry and basal shear stress (GlapTop2), or the mass balance or ice flow (HF) of the glacier. GlapTop2 is based on the perfect plasticity assumption (Nye, 1952), which was formulated for actively deforming glaciers. The central parameters for GlapTop2 are surface slope and basal shear stress τ (Paul & Linsbauer, 2012). Thus, this approach assumes that the glacier is in a condition in which basal shear stress is near the yield stress (Clarke et al., 2009), which is more probable for glaciers near to equilibrium conditions with significant ice flow. To overcome some of the restrictions of the perfect plasticity assumption, some authors have proposed a slope correction or an individual adjustment of f (Carrivick et al., 2016; James & Carrivick, 2016; Li et al., 2012). The HF model explicitly requires ice flow dynamics to grant mass conservation between the elevation bands (Huss & Farinotti, 2012). Surface slope of glaciers is central to both modelling approaches and also other more qualitative approaches like the manual criteria analysis to detect GBOs proposed by Frey et al. (2010a). GBO detection in the glacier bed relies on the assumption that the surface of current glaciers represents a smoothed copy of the subglacial topography (Frey et al., 2010a; Paul & Linsbauer, 2012). The subglacial topography composed of irregularities, zones of variable roughness and steepness, and GBOs impacts on the flow behaviour and the ice stress field (Sanders et al., 2010). Ice reacts to these impacts by deformation and compressive or extensive flow, illustrated by the formation of crevasses or ogives for example. Thus, ice flow and subglacial topography affect the shape of the glacier surface. In the case of cirque glaciers that experience strong downwasting, ice flow is strongly altered by negative mass balances, leading to a slowdown of glacier velocities, and by the shape of the subsurface (Dehecq et al., 2019; Sanders et al., 2018). Increasing debris cover, shading effects of surrounding cliffs and the topography are important factors that affect mass turnover and flow dynamics (Cuffey & Paterson, 2010). Hence, the surface of cirque and niche glaciers often does not necessarily reflect the subglacial bedrock well, challenging the assumption of a glacier surface representing the glacier bed. These factors vary significantly between valley and cirque glaciers and even more for ice sheets. With respect to the shallow ice approximation, this becomes most apparent when considering the longitudinal and lateral stresses. The smaller the glacier is, the more differences to the assumptions postulated within the shallow ice approximation arise owing to a more and more dominating lateral drag

and thus longitudinal stress regime (Sanders et al., 2010). Thus, the assumptions made by the ice thickness models, such as constant basal shear stress, are most probably met at valley glaciers rather than at small cirque glaciers (Haeberli & Hölzle, 1995; Viani et al., 2020). In consequence, the reliability of the GBO detection approach may be more successful for those depressions formed in the valley glaciers and less in the cirques.

Around 70% of the simulated GBOs are located in valley glaciers. Though these GBOs are not restricted to the tongue areas, this distribution indicates that larger glaciers may be closer to the idealised glacier condition that are assumed by the ice thickness models than smaller mountain glaciers. This distribution of potential GBOs, however, most probably underestimates potential future lakes in the cirques. Looking at the spatial distribution of high-alpine lakes, we can observe that the majority of lakes that formed after the Pleistocene glaciation are located in cirques and not in the valley floors (Buckel et al., 2018). Some of the glacier lakes that formed in valley floors may have disappeared in the meantime because of higher sediment delivery to valleys compared with the cirques induced by larges contributing areas. On the other hand, lakes that have evolved between the investigation periods mostly developed at the lower glacier margin of the glaciers, with a few exceptions at lateral glacier positions like at Goldbergkees glacier (Supplementary Figure 3). This observation may influence the validation of the approach using existing lakes. When lakes form at proglacial locations, their position within the glacier DEM used for modelling must have been at the margins of the glaciers. Slope values of the glacier surface may be higher at the margins compared with central parts of the glaciers because of glacier downwasting. Figure 9 plots slope angles of the glacier surface at the locations of simulated GBOs and the later exposed lakes. We observe up to 50% steeper inclination of the glacier surface at lake locations compared with locations where GBOs have been modelled (Figure 9). The slope analysis reveals that GBO modelling using GlapTop2 is more closely linked to low inclination zones of the glacier surface compared with HF. This effect may explain why the models show such a poor performance in predicting the true number of lakes, but also indicates that GBOs simulated within a distance to the glacier margin may be more reliable, compared with those directly positioned at the glacier front.

FIGURE 9 Plotting mean slope within the GBOs the glacier surface at the different modelling runs. The lakes column includes lakes that evolved between G11 and G13. We computed the slope area of these lake locations using the DEM of G11



6 | CONCLUSIONS

We simulated the bedrock topography underneath glaciers in the Austrian Alps using two different ice thickness models in order to detect locations of glacier bed overdeepenings. Our simulations were performed at two periods of glacier extent with glaciers dominated by cirque and niche types. The results indicate large differences in model performance between GlapTop2 and HF concerning the total ice volume and the number and geometry of simulated GBOs. The number and total area of the modelled GBOs are significantly overestimated by all models compared with the number of lakes that have evolved in the past. In comparison with high-resolution geophysical data, large discrepancies between models and field measurements are apparent in shape and location of the subglacial topography. Even though some of the observed GBOs underneath the existing glaciers have been reproduced by the models, their shape and volume were not met by the models. This indicates that the modelling approach in general is capable of indicating potential GBOs, but a prediction of their geometry is not reliable. We rank the HF model higher with respect to the shape and location of the bedrock, but less performant concerning the number of GBOs. GlapTop2 generated a significantly lower total ice volume and in general too high subsurface bedrock locations, but more consistent GBO locations between the model runs.

We compared GBOs modelled for two glacier extents with lakes that evolved within the time between the two extents. This analysis revealed very low matching for all model runs. Various factors influence these observations, including uncertainties in the comparisons between existing lakes and GBOs as well as potential shortcomings in GBO modelling at glacier margins. We could show that, even though glacier slope is a central parameter of the models, the range of slope within the area of simulated GBOs is high. This indicates that surface characteristics alone do not sufficiently predict potential GBOs. The reliability of the GBO detection approach may be higher for those depressions simulated in the tongue area but with a sufficient distance to the glacier margin and lower for those located within the cirques.

We relate the limited modelling performance to potential shortcomings of fundamental assumptions on glacier conditions by the models with respect to the type of glaciers. Both models assume vital glacier conditions characterised by a flow-driven glacier surface. Glaciers in the study area are much smaller compared with many other mountain areas and heavily affected by climate warming. We argue that cirque glaciers are not at all fulfilling the assumption of the shallow ice approximation, which is in accordance with other studies (Sanders et al., 2010). We assume that mass turnover of degrading cirque glaciers is low and that surfaces of downwasting cirque glaciers are often dominated by processes other than pure glacier flow. Hence, we consider some of the fundamental implications of the flow driven ice thickness models are not met by our glaciers. The ice thickness models perform better on large valley type glaciers and less well on cirque and niche glaciers. Even though more than 90% of the glaciers investigated here are mountain glaciers, GBOs are simulated mainly within valley glaciers. This mismatches with the overall occurrence of postglacial lakes in alpine areas that are dominantly found in cirques.

For the Austrian Alps, the models simulated roughly 20–150 GBOs underneath the current glacier extent. Analysing the ensemble of all modelling runs indicates that 42 GBOs have the greatest probability of occurrence, despite uncertainties that persistent lakes will

indeed form in these depressions in the future. The potential new lakes are located within 23 glaciers only, with most of them simulated in some of the largest glaciers of Austria, including the Pasterzenkees and the Gepatschferner glacier. Modelled GBOs at these locations account for a total area of 2 km² of new lakes. However, considering a potential underestimation of GBOs within cirque glacier, the number of potential future lakes may be higher. Many of these potential new lakes will be located at higher altitudes compared with the existing lakes (Salerno et al., 2014). With respect to the occurrence of warming-related gravitational mass movements, this will lead to a decreasing distance between lakes and steep rockwall at uppermost locations, where potential hazard processes may occur. This indicates a localised increase in hazard potential for high-alpine zones affected by climate change induced by some of these future high-alpine lakes.

ACKNOWLEDGEMENTS

We thank two anonymous reviewers and an associate editor for supportive comments and advice that helped to improve the manuscript substantially. Johannes Buckel, Milena Kocher and Christopher Hausmann and a few others have provided valuable support in the preparation of the base data for this study. Their help is gratefully appreciated. Johannes Buckel is thanked for his support in gathering the GPR data on Schmiedingerkees. The study was supported financially by the Austrian Academy of Sciences within the *Futurelakes* project. We also thank Matthias Huss for providing resources and support of the HF model and Andrea Fischer and colleagues for sharing the glacier inventory data. A very fruitful discussion with Wilfried Haerberli during the runtime of the *Futurelakes* project significantly helped to sharpen our view on potential future alpine lakes. Funding of the study was provided by the Austrian Academy of Sciences (ÖAW). The support is recognised with appreciation.

CONFLICT OF INTEREST

The authors declare that there are no conflict of interests.

AUTHOR CONTRIBUTIONS

J.C.O. and M.K. designed the study and applied the funding. J.C.O. led the research project and did the data analysis. K.H. performed the HF modelling, G.H. wrote the Python code for the GlapTop2 model, D.B. contributed the geophysical data on Wurtenkees, Goldbergkees and Pasterzenkees. J.C.O. wrote the initial draft of the manuscript. All authors reviewed and edited the manuscript.

DATA AVAILABILITY STATEMENT

Data on simulated GBOs are available via Pangea.de.

ORCID

Jan-Christoph Otto  <https://orcid.org/0000-0002-4552-3011>

Kay Helfricht  <https://orcid.org/0000-0002-8843-7594>

Günther Prasicek  <https://orcid.org/0000-0002-9332-1625>

Daniel Binder  <https://orcid.org/0000-0002-9939-688X>

Markus Keuschnig  <https://orcid.org/0000-0001-6070-1042>

REFERENCES

Abermann, J., Kuhn, M. & Fischer, A. (2011) Climatic controls of glacier distribution and glacier changes in Austria. *Annals of Glaciology*, 52(59), 83–90. <https://doi.org/10.3189/172756411799096222>

- Abermann, J., Lambrecht, A., Fischer, A. & Kuhn, M. (2009) Quantifying changes and trends in glacier area and volume in the Austrian Ötztal Alps (1969–1997–2006). *The Cryosphere*, 3(2), 205–215. <https://doi.org/10.5194/tc-3-205-2009>
- Allen, S.K., Linsbauer, A., Randhawa, S.S., Huggel, C., Rana, P. & Kumari, A. (2016) Glacial lake outburst flood risk in Himachal Pradesh, India: An integrative and anticipatory approach considering current and future threats. *Natural Hazards*, 84(3), 1741–1763. <https://doi.org/10.1007/s11069-016-2511-x>
- Andreassen, L.M., Huss, M., Melvold, K., Elvehøy, H. & Winsvold, S.H. (2015) Ice thickness measurements and volume estimates for glaciers in Norway. *Journal of Glaciology*, 61(228), 763–775. <https://doi.org/10.3189/2015JoG14J161>
- Avian, M., Bauer, C., Schögl, M., Widhalm, B., Gutjahr, K.H., Paster, M. et al. (2020) The status of earth observation techniques in monitoring high mountain environments at the example of pasterze glacier, austria: Data, methods, accuracies, processes, and scales. *Remote Sensing*, 12(8), 1251. <https://doi.org/10.3390/RS12081251>
- Binder, D. (2009) Bestimmung der Eismächtigkeitsverteilung dreier Gletscher der Hohen Tauern auf Basis von Ground Penetrating Radar (GPR) Daten. In: 175 S., Ill., graf. Darst., Kt.
- Binder, D., Brückl, E., Roch, K.H., Behm, M., Schöner, W. & Hynek, B. (2009) Determination of total ice volume and ice-thickness distribution of two glaciers in the Hohe Tauern region, Eastern Alps, from GPR data. *Annals of Glaciology*, 50(51), 71–79. <https://doi.org/10.3189/172756409789097522>
- Binder, D., Schöner, W., Fischer, A., Hynek, B. & Weys, G. (2011) The Ice Distribution of the Pasterze Glacier – Interpolation Approaches. In *Int. Conference on the 125 Anniversary of Sonnbllick Observatory 'Climate Change in High Mountain Regions', August 28–September 1: Salzburg*.
- Buckel, J. & Otto, J.-C. (2018) The Austrian Glacier Inventory GI 4 (2015) in ArcGis (shapefile) format. In *Supplement to: Buckel, Johannes; Otto, Jan-Christoph; Prasicek, Günther; Keuschnig, Markus (2018): Glacial lakes in Austria - Distribution and formation since the Little Ice Age. Global and Planetary Change*, 164, 39–51. <https://doi.org/10.1016/j.gloplacha.2018.03.003.PANGAEA>
- Buckel, J., Otto, J.C., Prasicek, G. & Keuschnig, M. (2018) Glacial lakes in Austria – Distribution and formation since the Little Ice Age. *Global and Planetary Change*, 164, 39–51. <https://doi.org/10.1016/j.gloplacha.2018.03.003>
- Capt, M., Bosson, J.B., Fischer, M., Micheletti, N. & Lambiel, C. (2016) Decadal evolution of a very small heavily debris-covered glacier in an Alpine permafrost environment. *Journal of Glaciology*, 62(233), 535–551. <https://doi.org/10.1017/jog.2016.56>
- Carrivick, J.L., Davies, B.J., James, W.H.M., Quincey, D.J. & Glasser, N.F. (2016) Distributed ice thickness and glacier volume in southern South America. *Global and Planetary Change*, 146, 122–132. <https://doi.org/10.1016/j.gloplacha.2016.09.010>
- Carrivick, J.L. & Tweed, F.S. (2013) Proglacial lakes: Character, behaviour and geological importance. *Quaternary Science Reviews*, 78, 34–52. <https://doi.org/10.1016/j.quascirev.2013.07.028>
- Clague, J.J. & O'Connor, J.E. (2015) Chapter 14 - Glacier-Related Outburst Floods A2 - Shroder, John F. In: Haeberli, W. & Whiteman, C. (Eds.) *Snow and Ice-Related Hazards, Risks and Disasters*. Boston: Academic Press.
- Clarke, G.K.C., Berthier, E., Schoof, C.G. & Jarosch, A.H. (2009) Neural networks applied to estimating subglacial topography and glacier volume. *Journal of Climate*, 22(8), 2146–2160. <https://doi.org/10.1175/2008JCLI2572.1>
- Cogley, J.G., Arendt, A., Bauder, A., Braithwaite, R., Hock, R., Jansson, P. et al. (2010) Glossary of glacier mass balance and related terms.
- Colonia, D., Torres, J., Haeberli, W., Schauwecker, S., Braendle, E., Giraldez, C. & Cochachin, A. (2017) Compiling an inventory of glacier-bed overdeepenings and potential new lakes in de-glaciating areas of the Peruvian Andes. *Water*, 9, 336. <https://doi.org/10.3390/w9050336>
- Cook, S.J., Kougkoulos, I., Edwards, L.A., Dortch, J. & Hoffmann, D. (2016) Glacier change and glacial lake outburst flood risk in the Bolivian Andes. *The Cryosphere*, 10(5), 2399–2413. <https://doi.org/10.5194/tc-10-2399-2016>
- Cook, S.J. & Swift, D.A. (2012) Subglacial basins: Their origin and importance in glacial systems and landscapes. *Earth-Science Reviews*, 115(4), 332–372. <https://doi.org/10.1016/j.earscirev.2012.09.009>
- Cuffey, K.M. & Paterson, W.S.B. (2010) *The physics of glaciers*. London, Oxford, Boston: Academic Press.
- DeBeer, C.M. & Sharp, M.J. (2009) Topographic influences on recent changes of very small glaciers in the Monashee Mountains, British Columbia, Canada. *Journal of Glaciology*, 55(192), 691–700. <https://doi.org/10.3189/002214309789470851>
- Dehecq, A., Gourmelen, N., Gardner, A.S., Brun, F., Goldberg, D., Nienow, P.W. et al. (2019) Twenty-first century glacier slowdown driven by mass loss in High Mountain Asia. *Nature Geoscience*, 12(1), 22–27. <https://doi.org/10.1038/s41561-018-0271-9>
- Drenkhan F., Huggel C., Guardamino L., Haeberli W. (2019) Managing risks and future options from new lakes in the deglaciating Andes of Peru: The example of the Vilcanota-Urubamba basin. *Science of The Total Environment*, 665, 465–483. <https://doi.org/10.1016/j.scitotenv.2019.02.070>
- Emmer, A., Klimeš, J., Mergili, M., Vilímeck, V. & Cochachin, A. (2016) 882 lakes of the Cordillera Blanca: An inventory, classification, evolution and assessment of susceptibility to outburst floods. *Catena*, 147, 269–279. <https://doi.org/10.1016/j.catena.2016.07.032>
- Farinotti, D., Brinkerhoff, D.J., Clarke, G.K.C., Fürst, J.J., Frey, H., Gantayat, P. et al. (2017) How accurate are estimates of glacier ice thickness? Results from ITMIX, the Ice Thickness Models Intercomparison eXperiment. *The Cryosphere*, 11(2), 949–970. <https://doi.org/10.5194/tc-11-949-2017>
- Farinotti, D., Huss, M., Bauder, A. & Funk, M. (2009) An estimate of the glacier ice volume in the Swiss Alps. *Global and Planetary Change*, 68(3), 225–231. <https://doi.org/10.1016/j.gloplacha.2009.05.004>
- Farinotti, D., Huss, M., Fürst, J.J., Landmann, J., Machguth, H., Maussion, F. & Pandit, A. (2019) A consensus estimate for the ice thickness distribution of all glaciers on Earth. *Nature Geoscience*, 12(3), 168–173. <https://doi.org/10.1038/s41561-019-0300-3>
- Fischer, A. & Markl, G. (2008) Mass balance measurements on Hintereisferner, Kesselwandferner and Jamtalferner 2003 to 2006: Database and results. *Zeitschrift Fur Gletscherkunde Und Glazialgeologie*, 42, 47.
- Fischer, A., Seiser, B., Stocker-Waldhuber, M., Mitterer, C. & Abermann, J. (2015a) The Austrian Glacier Inventories GI 1 (1969), GI 2 (1998), GI 3 (2006), and GI LIA in ArcGIS (shapefile) format. PANGAEA. <https://doi.org/10.1594/PANGAEA.844988>
- Fischer, A., Seiser, B., Stocker Waldhuber, M., Mitterer, C. & Abermann, J. (2015b) Tracing glacier changes in Austria from the Little Ice Age to the present using a lidar-based high-resolution glacier inventory in Austria. *The Cryosphere*, 9(2), 753–766. <https://doi.org/10.5194/tc-9-753-2015>
- Fischer, A., Span, N., Kuhn, M., Helfricht, K., Stocker-Waldhuber, M., Seiser, B. et al. (2015) Ground-penetrating radar (GPR) point measurements of ice thickness in Austria. In PANGAEA.
- Fleischer, F., Otto, J.C., Junker, R.R. & Hölbling, D. (2021) Evolution of debris cover on glaciers of the Eastern Alps, Austria, between 1996 and 2015. *Earth Surface Processes and Landforms*, 46(9), 1673–1691. <https://doi.org/10.1002/esp.5065>
- Florentine, C., Harper, J. & Fagre, D. (2020) Parsing complex terrain controls on mountain glacier response to climate forcing. *Global and Planetary Change*, 191, 103209. <https://doi.org/10.1016/j.gloplacha.2020.103209>
- Frey, H., Haeberli, W., Linsbauer, A., Huggel, C. & Paul, F. (2010a) A multi-level strategy for anticipating future glacier lake formation and associated hazard potentials. *Natural Hazards and Earth System Sciences*, 10(2), 339–352. <https://doi.org/10.5194/nhess-10-339-2010M4-Citavi>
- Frey, H., Huggel, C., Paul, F., & Haeberli, W. (2010b) Automated detection of glacier lakes based on remote sensing in view of assessing

- associated hazard potentials. *Proceedings 10th international symposium on high mountain remote sensing cartography*: 23–30.
- Frey, H., Machguth, H., Huss, M., Huggel, C., Bajracharya, S., Bolch, T. et al. (2014) Estimating the volume of glaciers in the Himalayan-Karakoram region using different methods. *The Cryosphere*, 8(6), 2313–2333. <https://doi.org/10.5194/tc-8-2313-2014M4-Citavi>
- Gharehchahi, S., James, W.H.M., Bhardwaj, A., Jensen, J.L.R., Sam, L., Ballinger, T.J. & Butler, D.R. (2020) Glacier ice thickness estimation and future lake formation in Swiss Southwestern Alps – The Upper Rhône Catchment: A VOLTA Application. *Remote Sensing*, 12(20), 3443. <https://doi.org/10.3390/rs12203443>
- Haeberli, W., Buetler, M., Huggel, C., Friedli, T.L., Schaub, Y. & Schleiss, A. J. (2016) New lakes in deglaciating high-mountain regions – Opportunities and risks. *Climatic Change*, 139(2), 201–214. <https://doi.org/10.1007/s10584-016-1771-5>
- Haeberli, W. & Hölzle, M. (1995) Application of inventory data for estimating characteristics of and regional climate effects on mountain glaciers: A pilot study with the European Alps. *Annals of Glaciology*, 21, 206–212. <https://doi.org/10.3189/S0260305500015834>
- Haeberli, W., Schaub, Y. & Huggel, C. (2017) Increasing risks related to landslides from degrading permafrost into new lakes in de-glaciating mountain ranges. *Geomorphology*, 293, 405–417. <https://doi.org/10.1016/j.geomorph.2016.02.009>
- Helfricht, K., Huss, M., Fischer, A. & Otto, J.C. (2019) Calibrated ice thickness estimate for all glaciers in Austria. *Frontiers in Earth Science*, 7, 68. <https://doi.org/10.3389/feart.2019.00068>
- Huss, M. & Farinotti, D. (2012) Distributed ice thickness and volume of all glaciers around the globe. *Journal of Geophysical Research: Earth Surface*, 117, F04010. <https://doi.org/10.1029/2012JF002523>
- Hutchinson, M.F. (1989) A new procedure for gridding elevation and stream line data with automatic removal of spurious pits. *Journal of Hydrology*, 106(3–4), 211–232. [https://doi.org/10.1016/0022-1694\(89\)90073-5](https://doi.org/10.1016/0022-1694(89)90073-5)
- Hutter, K. (1983) The Application of the Shallow-Ice Approximation. In: *Theoretical Glaciology. Mathematical Approaches to Geophysics, vol 1*. Dordrecht: Springer. https://doi.org/10.1007/978-94-015-1167-4_5
- James, W.H. & Carrivick, J.L. (2016) Automated modelling of spatially-distributed glacier ice thickness and volume. *Computers & Geosciences*, 92, 90–103. <https://doi.org/10.1016/j.cageo.2016.04.007>
- Kapitsa, V., Shahgedanova, M., Machguth, H., Severskiy, I. & Medeu, A. (2017) Assessment of evolution and risks of glacier lake outbursts in the Djungarskiy Alatau, Central Asia, using Landsat imagery and glacier bed topography modelling. *Natural Hazards and Earth System Sciences*, 17(10), 1837–1856. <https://doi.org/10.5194/nhess-17-1837-2017>
- King, O., Bhattacharya, A., Bhambri, R. & Bolch, T. (2019) Glacial lakes exacerbate Himalayan glacier mass loss. *Scientific Reports*, 9(1), 18145. <https://doi.org/10.1038/s41598-019-53733-x>
- Lambrecht, A. & Kuhn, M. (2007) Glacier changes in the Austrian Alps during the last three decades, derived from the new Austrian glacier inventory. *Annals of Glaciology*, 46, 177–184. <https://doi.org/10.3189/172756407782871341>
- Laute, K. & Beylich, A.A. (2021) Recent glacier changes and formation of new proglacial lakes at the Jostedalbreen ice cap in southwest Norway. In: Beylich, A.A., *Landscapes and Landforms of Norway*, World Geomorphological Landscapes. Cham: Springer, 71–95. https://doi.org/10.1007/978-3-030-52563-7_4
- Li, H., Ng, F., Li, Z., Qin, D. & Cheng, G. (2012) An extended “perfect-plasticity” method for estimating ice thickness along the flow line of mountain glaciers. *Journal of Geophysical Research: Earth Surface*, 117(F1), F01020. <https://doi.org/10.1029/2011JF002104>
- Linsbauer, A., Frey, H., Haeberli, W., Machguth, H., Azam, M.F. & Allen, S. (2016) Modelling glacier-bed overdeepenings and possible future lakes for the glaciers in the Himalaya-Karakoram region. *Annals of Glaciology*, 57(71), 119–130. <https://doi.org/10.3189/2016AoG71A627>
- Linsbauer, A., Paul, F. & Haeberli, W. (2012) Modeling glacier thickness distribution and bed topography over entire mountain ranges with GlabTop: Application of a fast and robust approach. *Journal of Geophysical Research: Earth Surface*, 117(F3), F03007. <https://doi.org/10.1029/2011Jf002313>
- Linsbauer, A., Paul, F., Machguth, H. & Haeberli, W. (2013) Comparing three different methods to model scenarios of future glacier change in the Swiss Alps. *Annals of Glaciology*, 54(63), 241–253. <https://doi.org/10.3189/2013AoG63A400>
- Livingstone, S.J., Clark, C.D., Woodward, J. & Kingslake, J. (2013) Potential subglacial lake locations and meltwater drainage pathways beneath the Antarctic and Greenland ice sheets. *The Cryosphere*, 7(6), 1721–1740. <https://doi.org/10.5194/tc-7-1721-2013>
- Magnin, F., Haeberli, W., Linsbauer, A., Deline, P. & Ravelin, L. (2020) Estimating glacier-bed overdeepenings as possible sites of future lakes in the de-glaciating Mont Blanc massif (Western European Alps). *Geomorphology*, 350, 106913. <https://doi.org/10.1016/j.geomorph.2019.106913>
- Mergili, M., Müller, J.P. & Schneider, J.F. (2013) Spatio-temporal development of high-mountain lakes in the headwaters of the Amu Darya River (Central Asia). *Global and Planetary Change*, 107, 13–24. <https://doi.org/10.1016/j.gloplacha.2013.04.001>
- Nicolussi, K. & Patzelt, G. (2000) Discovery of early Holocene wood and peat on the forefield of the Pasterze Glacier, Eastern Alps, Austria. *The Holocene*, 10(2), 191–199. <https://doi.org/10.1191/09596830066855842>
- Nye, J. (1965) The flow of a glacier in a channel of rectangular, elliptic or parabolic cross-section. *Journal of Glaciology*, 5(41), 661–690. <https://doi.org/10.1017/S0022143000018670>
- Nye, J.F. (1952) The mechanics of glacier flow. *Journal of Glaciology*, 2(12), 82–93. <https://doi.org/10.3189/S0022143000033967>
- O'Connor, J.E. & Costa, J.E. (2004) The World's Largest Floods, Past and Present: Their Causes and Magnitudes. In: U.S. Geological Survey: Reston, Virginia; 19.
- Otto, J.-C. (2019) Proglacial Lakes in High Mountain Environments. In: Heckmann, T. & Morche, D. (Eds.) *Geomorphology of Proglacial Systems: Landform and Sediment Dynamics in Recently Deglaciating Alpine Landscapes*. Cham: Springer International Publishing.
- Otto, J.-C., Hausmann, C. & Fischer, A. (2018) Semi-automated classification of mountain glacier types. In *EGU General Assembly Conference Abstracts*; 6473.
- Paasche, Ø. (2011) Cirque Glaciers. In: Singh, V.P., Singh, P. & Haritashya, U.K. (Eds.) *Encyclopedia of Snow, Ice and Glaciers*. Dordrecht: Springer Netherlands.
- Pandey, P., Ali, S.N. & Champati Ray, P.K. (2021) Glacier-glacial lake interactions and glacial lake development in the Central Himalaya, India (1994–2017). *Journal of Earth Science*, <https://doi.org/10.1007/s12583-020-1056-9>
- Pandit, A. & Ramsankaran, R. (2020) Identification of potential sites for future lake formation and expansion of existing lakes in glaciers of Chandra Basin, Western Himalayas, India. *Frontiers in Earth Science*, 8, 500116. <https://doi.org/10.3389/feart.2020.500116>
- Patzelt, G. (2013) Austrian glacier inventory 1969 (G I). PANGAEA, <https://doi.org/10.1594/PANGAEA.807098>
- Paul, F. & Linsbauer, A. (2012) Modeling of glacier bed topography from glacier outlines, central branch lines, and a DEM. *International Journal of Geographical Information Science*, 26(7), 1173–1190. <https://doi.org/10.1080/13658816.2011.627859>
- Pelto, B.M., Maussion, F., Menounos, B., Radić, V. & Zeuner, M. (2020) Bias-corrected estimates of glacier thickness in the Columbia River Basin, Canada. *Journal of Glaciology*, 66(260), 1051–1063. <https://doi.org/10.1017/jog.2020.75>
- Pelto, M., Capps, D., Clague, J.J. & Pelto, B. (2013) Rising ELA and expanding proglacial lakes indicate impending rapid retreat of Brady Glacier, Alaska. *Hydrological Processes*, 27(21), 3075–3082. <https://doi.org/10.1002/hyp.9913>
- Pfeffer, W.T., Arendt, A.A., Bliss, A., Bolch, T., Cogley, J.G., Gardner, A.S. et al. (2014) The Randolph Glacier Inventory: a globally complete inventory of glaciers. *Journal of Glaciology*, 60(221), 537–552. <https://doi.org/10.3189/2014JoG13J176>

- Pierre KAS., Louis, VLS., Schiff, SL., Lehnher, I., Dainard, PG., Gardner, AS. et al. (2019) Proglacial freshwaters are significant and previously unrecognized sinks of atmospheric CO₂. *Proceedings of the National Academy of Sciences*, 116, 17690–17695. <https://doi.org/10.1073/pnas.1904241116>
- Ramsankaran, R., Pandit, A. & Azam, M.F. (2018) Spatially distributed ice-thickness modelling for Chhota Shigri Glacier in western Himalayas, India. *International Journal of Remote Sensing*, 39(10), 3320–3343. <https://doi.org/10.1080/01431161.2018.1441563>
- RGI Consortium. (2017) Randolph glacier inventory – A dataset of global glacier outlines: version 6.0. *Global Land Ice Measurements from Space, Colorado, USA, Tech. Rep.*
- Salerno, F., Gambelli, S., Viviano, G., Thakuri, S., Guyennon, N., D'Agata, C. et al. (2014) High alpine ponds shift upwards as average temperatures increase: A case study of the Ortles–Cevedale mountain group (Southern Alps, Italy) over the last 50 years. *Global and Planetary Change*, 120, 81–91. <https://doi.org/10.1016/j.gloplacha.2014.06.003>
- Sanders, J.W., Cuffey, K.M., Macgregor, K.R., Kavanaugh, J.L. & Dow, C.F. (2010) Dynamics of an alpine cirque glacier. *American Journal of Science*, 310(8), 753–773. <https://doi.org/10.2475/08.2010.03>
- Sanders, J.W., Cuffey, K.M., MacGregor, K.R., Kavanaugh, J.L. & Dow, C.F. (2018) Variations in the surface velocity of an alpine cirque glacier. *Journal of Glaciology*, 64(248), 969–976. <https://doi.org/10.1017/jog.2018.85>
- Slupetzky, H. (1993) Holzfunde aus dem Vorfeld der Pasterze. Erste Ergebnisse von 14C-Datierungen. *Zeitschrift für Gletscherkunde und Glazialgeologie*, 26, 179–187.
- Sommer, C., Malz, P., Seehaus, T.C., Lippl, S., Zemp, M. & Braun, M.H. (2020) Rapid glacier retreat and downwasting throughout the European Alps in the early 21st century. *Nature Communications*, 11(1), 3209. <https://doi.org/10.1038/s41467-020-16818-0>
- Song, C., Sheng, Y., Ke, L., Nie, Y. & Wang, J. (2016) Glacial lake evolution in the southeastern Tibetan Plateau and the cause of rapid expansion of proglacial lakes linked to glacial-hydrogeomorphic processes. *Journal of Hydrology*, 540, 504–514. <https://doi.org/10.1016/j.jhydrol.2016.06.054>
- Span, N., Fischer, A., Kuhn, M., Massimo, M. & Butschek, M. (2005) Radarmessungen der Eisdicke Österreichischer Gletscher. *Österreichische Beiträge zur Meteorologie und Geophysik*, 33, 146.
- Stocker-Waldhuber, M., Fischer, A., Helfricht, K. & Kuhn, M. (2019) Long-term records of glacier surface velocities in the Ötztal Alps (Austria). *Earth System Science Data*, 11(2), 705–715. <https://doi.org/10.5194/essd-11-705-2019>
- Sutherland, J.L., Carrivick, J.L., Gandy, N., Shulmeister, J., Quincey, D.J. & Cornford, S.L. (2020) Proglacial lakes control glacier geometry and behavior during recession. *Geophysical Research Letters*, 47, e2020GL088865. <https://doi.org/10.1029/2020GL088865>
- Viani, C., Machguth, H., Huggel, C., Godio, A., Franco, D., Perotti, L. & Giardino, M. (2020) Potential future lakes from continued glacier shrinkage in the Aosta Valley Region (Western Alps, Italy). *Geomorphology*, 355, 107068. <https://doi.org/10.1016/j.geomorph.2020.107068>
- Wilson, R., Glasser, N.F., Reynolds, J.M., Harrison, S., Anaconda, P.I., Schaefer, M. & Shannon, S. (2018) Glacial lakes of the Central and Patagonian Andes. *Global and Planetary Change*, 162, 275–291. <https://doi.org/10.1016/j.gloplacha.2018.01.004>
- Zhang, G., Bolch, T., Allen, S., Linsbauer, A., Chen, W. & Wang, W. (2019) Glacial lake evolution and glacier–lake interactions in the Poiqu River basin, central Himalaya, 1964–2017. *Journal of Glaciology*, 65(251), 347–365. <https://doi.org/10.1017/jog.2019.13>
- Zhang, G., Yao, T., Xie, H., Wang, W. & Yang, W. (2015) An inventory of glacial lakes in the Third Pole region and their changes in response to global warming. *Global and Planetary Change*, 131, 148–157. <https://doi.org/10.1016/j.gloplacha.2015.05.013>

SUPPORTING INFORMATION

Additional supporting information may be found in the online version of the article at the publisher's website.

How to cite this article: Otto, J.-C., Helfricht, K., Prasicsek, G., Binder, D. & Keuschnig, M. (2021) Testing the performance of ice thickness models to estimate the formation of potential future glacial lakes in Austria. *Earth Surface Processes and Landforms*, 1–19. Available from: <https://doi.org/10.1002/esp.5266>